

Review

Red Supergiants in the Milky Way and Nearby Galaxies

Alceste Z. Bonanos 

Institute for Astronomy, Astrophysics, Space Applications and Remote Sensing, National Observatory of Athens, GR-15326 Penteli, Greece; bonanos@astro.noa.gr

Abstract: Identifications of red supergiants (RSGs) in the Milky Way and nearby galaxies have experienced an exponential increase in recent years, driven by advancements in selection techniques, the continued expansion of archival datasets, and a steady increase in spectroscopic data. This review describes the advances in methodologies and selection criteria for identifying RSGs and presents the current census of these stars in our own Galaxy and nearby galaxies. It also describes the insights gained from resolving nearby RSGs and their complex circumstellar material in the Milky Way and from the growing samples of RSGs being discovered in the Local Group and beyond. These advances impact the Humphreys–Davidson limit in the cool part of the Hertzsprung–Russell diagram. Furthermore, they provide insight into extreme RSGs and the role of photometric variability and, in particular, of the newly discovered phenomenon of dimming events. Recent observations have enabled the determination of the binarity fraction among RSGs, offering new constraints to stellar evolution. Looking ahead, the synergy between large-scale surveys, high-resolution observations, and emerging machine-learning tools promises to further transform our understanding of the final evolutionary stages of massive stars in the coming decade.

Keywords: stars: massive; supergiants; stars: late-type; stars: evolution; stars: mass loss; stars: winds, outflows

1. Introduction

Over the last decade, there has been significant progress enabling in-depth studies of individual RSGs and the characterization of entire RSG populations in nearby galaxies. Improved instrumentation has led to the availability of multi-band photometric catalogs of nearby galaxies and time-series photometry of thousands of stars in the Galaxy, reaching out to several Mpc, while multi-object spectroscopy has enabled detailed studies of hundreds of RSGs in both the optical and near-infrared. This has allowed for a comprehensive view of RSGs, ranging from the lowest luminosities ($\log L/L_{\odot} \sim 4$) to the Humphreys–Davidson limit [1] at $\log L/L_{\odot} \sim 5.8$. We have entered the era of large RSG samples, which enable us to tackle open questions regarding their evolution, wind driving mechanism, mass-loss rates, and variability. We can also resolve RSGs and learn about their mass-loss history. The following sections review the improvements and limitations of the selection criteria and recent studies of the RSG population of the Milky Way, the Local Group, and beyond. The final sections present insights gained from extragalactic RSGs and a future outlook.

2. Selection Criteria

The first step in investigating RSGs requires robust selection criteria to identify the objects of interest and distinguish them from contaminants, such as red dwarfs, red giants, distant red galaxies, or other reddened objects. The initial studies, dating back to the 1970s, confirmed RSGs by obtaining long-slit spectra of candidates (resulting from objective-prism studies or color criteria) in the region of the CaII triplet, e.g., [2], or in the blue, e.g., [3]. Significant progress has been made over the last three decades in improving the selection criteria and making them broadly applicable, although spectra are still required to confirm the classification.

arXiv:2507.15964v1 [astro-ph.GA] 21 Jul 2025



Citation: Bonanos, A.Z. Red Supergiants in the Milky Way and Nearby Galaxies. *Galaxies* **2025**, *13*, 66. <https://doi.org/10.3390/galaxies13030066>

Received: 4 April 2025

Revised: 27 May 2025

Accepted: 30 May 2025

Published: 5 June 2025



Copyright: © 2025 by the author. Licensee MDPI, Basel, Switzerland. This article is an open access article distributed under the terms and conditions of the Creative Commons Attribution (CC BY) license (<https://creativecommons.org/licenses/by/4.0/>).

In 1998, Massey [4] discovered that low surface gravity red stars separate from red dwarfs on a $B - V$ vs. $V - R$ color diagram, providing the first selection criteria to identify the RSG population in nearby galaxies. This discovery stemmed from the multi-band survey of Local Group galaxies undertaken by Massey and collaborators in 1999–2001 using the Curtis Schmidt telescope for the Magellanic Clouds [5] (with its wide-field CCDs) and the KPNO and CTIO 4 m telescopes for more distant Local Group galaxies [6]. However, foreground stars remained a contaminant and spectroscopy was considered and still remains the most reliable way to confirm an RSG candidate. Furthermore, red giant and intermediate-mass AGB stars appear similar spectroscopically, see, e.g., [7,8]; therefore, distinguishing RSGs from these types of stars is challenging. Massey and Olsen [9] were the first to use multi-object spectroscopy to study a population of over 100 RSGs in the LMC and SMC, finding a contamination fraction by foreground red dwarfs of 5% and 11%, respectively. Subsequent surveys of the Magellanic Clouds M31 and M33 (see Section 4) obtained spectroscopy (in particular of the CaII triplet region) and used radial velocities to distinguish red foreground stars from RSGs in the target galaxies.

The next breakthrough came with the 2MASS all-sky survey. As the RSG spectral energy distribution peaks in the near-IR, the IR regime was the next obvious region to develop selection criteria in. The infrared reddening-free parameter $Q = (J - H) - 1.8 \times (H - K_s)$ (see, e.g., [10]) was used to select RSGs as stars with $Q = 0.1$ – 0.4 , primarily in the Milky Way (see, e.g., [11]). Furthermore, color-cuts in color–magnitude and color–color diagrams using $V - K$, $J - H$, and $H - K$ were developed to identify RSG candidates and distinguish them from red giants and asymptotic giant branch (AGB) stars. Yang et al. [12] demonstrated that AGB stars can be distinguished from RSG using near-IR colors, while Yang et al. [13] demonstrated the separation of low and high surface gravity stars using the H -bump at $1.6 \mu\text{m}$. Moreover, the metallicity dependence of the optical and near-IR colors of RSGs has been explored in Li et al. [14]. In Figure 1, the RSG branch is distinct from the AGB branch and seems to extend to luminosities below the nominal cut-off at $M_{K_s} = -7$ mag, indicating a sequence of red He-burning stars, which extends below the “massive star” definition to intermediate mass stars. This raises the question of what the definition of a RSG should be and whether or not the requirement of core-collapse should be included. Yang et al. [15] investigated the lowest luminosity and mass limit of RSGs, finding it to extend down to $\log L/L_{\odot} \sim 3.5$ and an initial mass $\sim 6 M_{\odot}$.

The advent of *Spitzer* and its Legacy surveys of the Magellanic Clouds [16,17] lead to mid-IR “roadmaps” for interpreting luminous massive stars [18,19]. RSGs were found to be among the brightest mid-IR sources, due to their intrinsic brightness and due to being surrounded by their own dust. This enabled the development of new mid-IR criteria (e.g., $[3.6]$ – $[4.5]$ and $J - [3.6]$ vs. $[3.6]$) to identify RSGs and in particular dusty RSGs (with $[3.6]$ – $[4.5] > 0.1$ mag), as circumstellar dust surrounding RSGs produces excess infrared emissions. The fact that the majority of RSGs have mid-IR colors $[3.6]$ – $[4.5] \leq 0$ (see Figure 2) are likely due to the presence of CO and SiO bands in these stars affecting the $[4.5]$ band [20], while RSGs with high mass-loss rates exhibit increased crystalline silicates [21]. The *WISE* and *NEOWISE* missions have also produced mid-IR data for the whole sky; however, their resolution limits the application of the mid-IR criteria with *WISE* to our Milky Way. A combination of near- and mid-IR criteria was suggested by Messineo et al. [22] for the Galactic plane. The mid-IR criteria have proven successful in selecting dusty massive stars [23]. However, they picked up HII regions, LBVs, sgB[e] stars, and emission objects as contaminants. The methodology was improved by the ASSESS project [24], which also considered the optical counterparts, as well as a visual check to reject extended sources (e.g., galaxies) using archival images, yielding a success rate of 36% in selecting evolved massive stars. Furthermore, ASSESS demonstrated that RSGs with IR excess $[3.6]$ – $[4.5] > 0.1$ mag have undergone episodic mass loss. Currently, JWST, which can only survey portions of nearby galaxies given its small field of view, is providing very deep, high-resolution images and accurate near- and mid-IR photometry for galaxies at ~ 10 Mpc (e.g., PHANGS-JWST [25,26]), at a similar quality as the performance of *Spitzer* at 1 Mpc, since the angular

resolution of JWST is ~ 10 times better. Levesque [27] have investigated near-IR diagnostics for selecting RSGs from foreground sources, while Boyer et al. [28] investigated color-color diagrams with JWST filters in the range between 0.9 and 4.3 μm to separate RSGs from AGB stars in the Wolf–Lundmark–Melotte (WLM) galaxy. Spiral galaxies beyond about 10 Mpc can fit in the field of view of JWST; therefore, JWST is well suited to detect and characterize entire populations of RSGs in a variety of environments and metallicities.

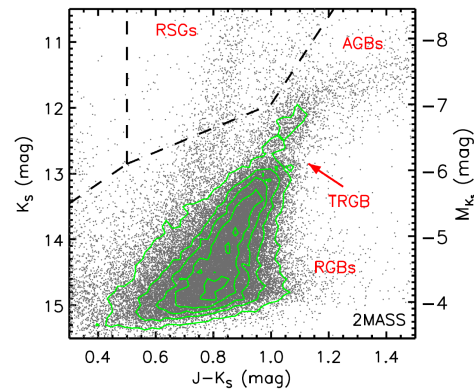


Figure 1. Separation of RSG from AGB in K_s vs. $J - K_s$ CMD in the SMC (reproduced from [12]). The dashed lines indicate the proposed criteria for distinguishing RSGs.

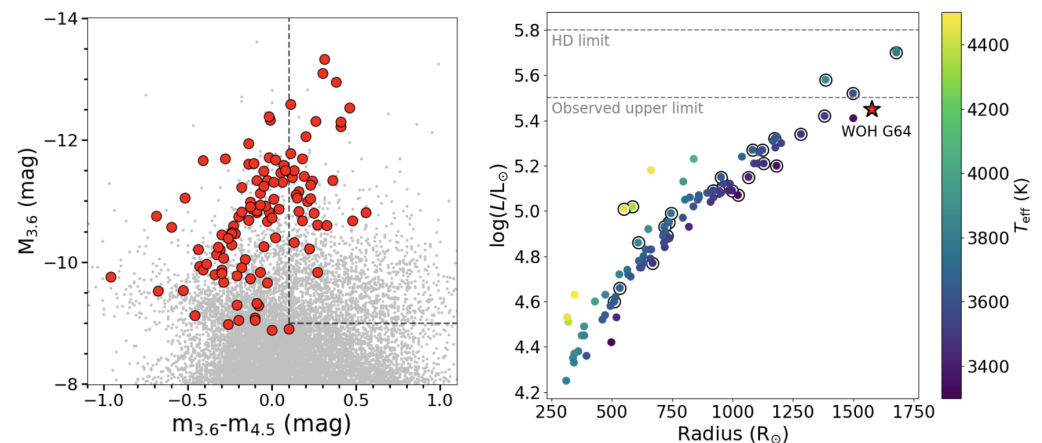


Figure 2. (Left): $[3.6]-[4.5]$ vs. $M_{[3.6]}$ color-magnitude diagrams of 129 RSGs in nearby galaxies from the ASSESS project [24]. Gray background points are sources from the *Spitzer* point source catalog of NGC 300. The dashed lines indicate the region of prioritized sources exhibiting IR excess, a sign of episodic mass loss. (Right): Stellar radius versus luminosity for 92 of those RSGs that have a luminosity determination. Circles indicate sources from the dusty sample, four of which (including three dusty ones) exceed the observed upper limit. The extreme RSG WOH G64 is marked by a red star. (reproduced from [29]).

The *Gaia* mission has measured proper motions and parallaxes for billions of stars (in data releases DR2 and DR3 [30–32]), providing a way to eliminate or at least greatly reduce foreground red giants, which plagued previous methodologies, and have led to a great improvement in the selection criteria. Aadland et al. [33] were the first to apply *Gaia* parallaxes to eliminate foreground stars in the direction of the LMC. Yang et al. [12] and Maravelias et al. [34] similarly performed *Gaia* cleaning to eliminate foreground stars toward the SMC and M31 and M33, respectively, by modeling the proper motion distribution of the foreground vs. host galaxy stars. This method was applied in Bonanos et al. [24] and de Wit et al. [35] to select dusty RSGs in nearby galaxies and helped reduce the foreground contamination (to 13%). *Gaia* also provided low-resolution spectra, which have been ex-

ploited to determine classification criteria based on the spectral features near the calcium triplet [36], to search for RSGs [37,38], and as a training set for deriving the parameters of RSGs with machine learning [39].

During the last few years, machine-learning techniques have emerged as a very promising method to identify RSGs in nearby galaxies to distances beyond 10 Mpc. Dorn-Wallenstein et al. [40] and Maravelias et al. [34] were the first to apply machine-learning techniques and develop algorithms to classify evolved massive stars. These two independent studies were both based on optical and infrared color indexes (the former also included photometric variability from the infrared light curves), and both found their algorithms to have a success rate of recovering RSGs that is over 90%. Maravelias et al. [41] has applied the algorithm to over 1 million sources in 26 nearby galaxies within 5 Mpc, producing accurate classifications for over 275,000 sources. These include over 120,000 RSGs and likely contain the entire RSG population of M31, M33, NGC 6822, and IC 1613. As the input data improve with the increasing amount of JWST data of nearby galaxies becoming available, and soon data from Rubin LSST, these algorithms will be able to achieve even higher success in identifying RSGs.

An underexploited tool for selecting RSGs is time-series photometry, as RSGs exhibit semi-regular or irregular variability, with a typical amplitude of ~ 1 mag in the optical, and in extreme cases up to 4 mag [42,43], while in the mid-infrared the amplitudes are typically up to 0.5 mag [44]. Variability in RSGs is due to both the pulsations and motions of large convective cells, while the extreme cases suggest a superwind phase. The amplitude of optical variability correlates with luminosity, e.g., [45]; moreover, a period–luminosity relation has been established in various bands [46–48], with the *K*-band having the least scatter. Granulation, which appears on the surface of RSGs due to the motion of convective cells and manifests as irregular variability, was presented as a new method for identifying and probing the properties of RSGs by Ren and Jiang [49]. They analyzed the light curves of a large sample of RSGs and found characteristic amplitudes of 10–1000 mmag and evolution timescales of the granulations between several days to 1 yr. These quantities were also shown to increase with metallicity and to correlate with the physical properties of the RSGs, demonstrating the importance of variability as a tool to study RSGs. The recent availability of optical data from transient surveys such as PanSTARRS1, ATLAS, ZTF, and *Gaia* (and in particular, *Gaia* DR4 expected in 2026) and mid-infrared light curves from AllWISE and NEOWISE allow variability information to be considered in a systematic way in the identification of RSGs. Within the next decade, high-cadence observations will become available for thousands of RSGs in nearby galaxies, launching a time-domain revolution in studies of evolved massive stars, and in particular, RSGs.

Once identified, optical and near-IR RSG spectra can be obtained and classified using the atlases of Rayner et al. [8] or Messineo et al. [50], and physical parameters can be extracted. This is currently feasible only for RSGs within a few Mpc, given the limiting magnitude achievable with existing instrumentation on 10 m class telescopes. The effective temperature, T_{eff} , can be derived from the spectra using 1D MARCS models [51], corrected for non-local thermal equilibrium effects [52–54], or alternatively by using empirical or synthetic relations based on $J - K_s$ colors, e.g., [29]. The luminosities (L) can be obtained via SED fitting (or metallicity-dependent bolometric corrections in the *K*-band, BC_K). The radii (R) can then be derived from the Stefan–Boltzmann law.

3. RSG Population of the Milky Way

The RSG population of the Milky Way remains largely unexplored. This is because the discovery and characterization of RSGs in our Galaxy faces two obstacles: high extinction values and uncertain distances. RSGs are mainly found in OB associations and clusters that are located in the Galactic disk; therefore, extinction becomes an increasing problem with distance. The case of Betelgeuse illustrates the distance issue: despite being the brightest, most well-known and possibly the most well-studied (with >150 refereed publications including ‘Betelgeuse’ in the title) RSG in the sky, its uncertain distance and wavelength-

dependent angular diameter, e.g., [55–57], affect the interpretation of the observations. Current distance estimates range from 168_{-15}^{+27} pc (based on a seismic analysis [58]) to 222_{-34}^{+48} pc (based on an updated astrometric solution [59]). This distance range translates to a range in radii between 750 and 1000 R_{\odot} .

Systematic searches for RSGs in the Milky Way began with the onset of near-IR surveys. Massive clusters containing RSGs were identified by selecting groups of bright stars, leading to the discovery of several clusters rich in supergiants, e.g., [11,60–63], located at the base of the Scutum–Crux arm near its interface with the Galactic Bar (see also [64]). RSGs have been discovered in open clusters, e.g., the coeval cluster NGC 7419 [65] and super star clusters, such as Westerlund 1 [66] and the Galactic Center (GCIRS7 [67]), as well as in the Perseus arm [68] and the Per OB1 association [69,70]. Healy et al. [71] performed a comprehensive study of RSGs in the Milky Way, which extended to 12.9 kpc and included 578 highly probable RSGs. This is only a small fraction of RSGs in the Milky Way. The total number was estimated to be ~ 5000 by Gehrz [72], but more recently was increased to over 11,000 RSG candidates by Zhang et al. [38]. These candidates were identified by combining low-resolution *Gaia* spectra with color criteria, and therefore the number is expected to be more accurate. Zhang et al. [73] identified over 450 new, low-luminosity RSGs in the Milky Way out to 30 kpc (see Figure 3) by analyzing the granulation characteristics of OGLE light curves, in combination with *Gaia* DR3 parameters to eliminate red giant branch stars.

The RSGs in our Galaxy offer us the opportunity for detailed studies of the circumstellar environment, and in particular of the mass-loss events that have occurred in their recent history. The nearest RSGs can be resolved with high-resolution imaging using, e.g., *HST*, e.g., VY CMa [74], NACO, and SPHERE on VLT, e.g., Betelgeuse [75,76], the MMT, and *SOFIA*, e.g., [77,78] and interferometry, using, for example, GRAVITY or MATISSE on the VLT interferometer, e.g., [76,79], ALMA, e.g., VY Canis Majoris [80] or CHARA, e.g., *H*-band interferometry of AZ Cyg and RW Cep [81–83]. Such high-resolution imaging observations have revealed complex circumstellar media, implying multiple asymmetric ejections, e.g., VY CMa [74]; see Figure 4. In addition, bow shocks have been discovered around several RSGs in the Milky Way: Betelgeuse [84] (see Figure 4), μ Cephei [85], IRC –10414 [86], and W237 in Westerlund 1 with JWST [87]. Evidence for a bow shock around the luminous RSG [W60] B90 in the LMC was presented by Munoz-Sanchez et al. [88], making it the first extragalactic RSG with a bow shock and a massive analog of Betelgeuse.

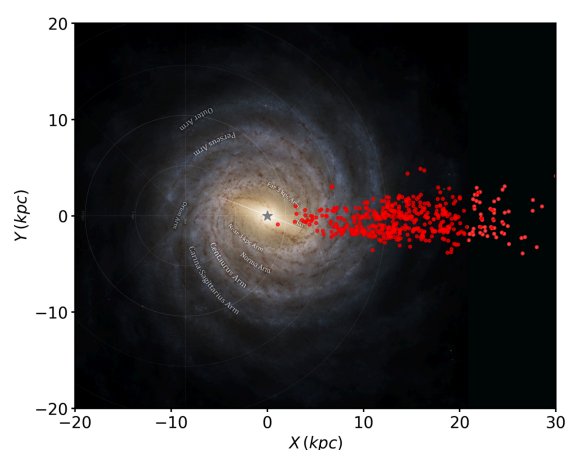


Figure 3. Distribution of new, low-luminosity RSGs identified out to 30 kpc using the granulation characteristics of OGLE light curves (reproduced from [73]).

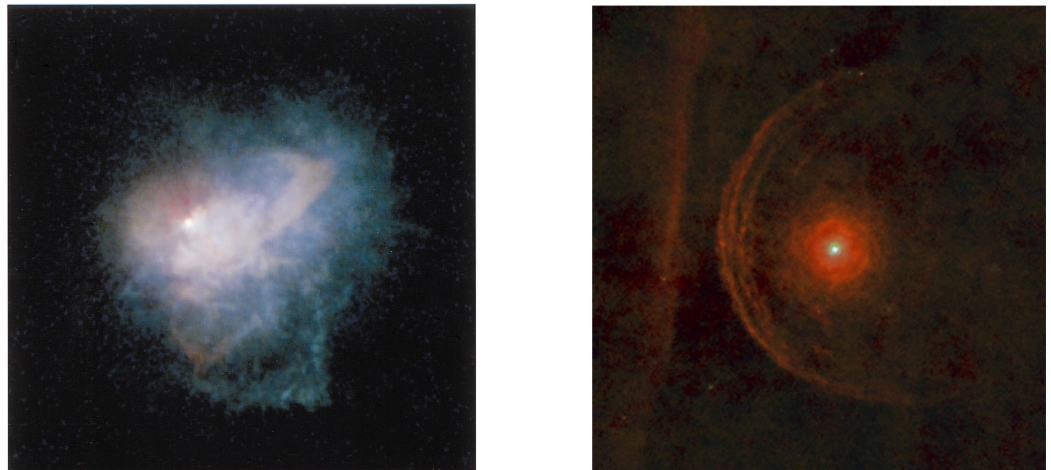


Figure 4. Examples of resolved RSGs in the Milky Way. **Left:** *HST* composite image of VY CMa revealing the structure of its circumstellar material (reproduced from [74]). **Right:** Bow shock and bar feature of Betelgeuse resolved with *Herschel* [Image credit: ESA/*Herschel*/PACS/MESS].

Galactic RSGs have also been crucial in the determination of the RSG mass-loss rates. Beasor et al. [89] used coeval RSGs in open clusters to derive their mass-loss rates and a steep mass-loss rate relation with luminosity, as a function of initial mass. They found much lower mass-loss rates than previous studies, implying that quiescent mass loss cannot strip the hydrogen envelopes of RSGs, therefore, affecting their evolution. Decin et al. [90] resolved 5 RSGs with ALMA and measured independent, gas mass-loss rates based on CO(2–1). Antoniadis et al. [91] managed to reconcile the dust and gas mass-loss rates, confirming the lower values found from these studies. This topic is reviewed in the chapter by van Loon in this Special Issue. Finally, the topic of RSG binaries in our Galaxy is reviewed in the introductory chapter by Humphreys.

4. RSG Population of the Local Group

The Local Group galaxies contain stars at a large range of metallicities, from $Z = 0.06 Z_{\odot}$ in Sextans A [92] and $0.14 Z_{\odot}$ in WLM [93] to $1.5 Z_{\odot}$ in M31 [94]. Moreover, the galaxies of the Local Group do not suffer from the distance uncertainties and high extinction that plague studies of the RSGs in the Milky Way. Distances to these galaxies are relatively well measured; for example, detached eclipsing binaries have provided a 1% distance to the LMC [95], while the Cepheid period–luminosity relation [96] and the tip of the red giant branch method [97] have provided uniform and accurate distances with typical statistical errors of $\sim 5\%$ (total errors including systematics are larger) for most of the galaxies in the Local Group (except for M33, see, e.g., [98]) and beyond. Armed with accurate distances, the availability of accurate optical and, in particular, near-IR photometry from wide-field surveys to eliminate giants and *Gaia* data to remove foreground sources, the RSG population of the galaxies in the Local Group has started to emerge.

As mentioned above, the wide-field *UBVR* CCD surveys of the Magellanic Clouds by Massey [5], the *UBVRI* survey of M31 and M33 by Massey et al. [99], and of seven dwarf galaxies—IC 10, NGC 6822, WLM, Sextans B, Sextans A, Pegasus, and Phoenix—by Massey et al. [6] provided the first photometric catalogs for basing the selection of RSGs in the Local Group. The availability of multi-object slit or fiber spectrographs enabled follow-up spectroscopy for hundreds of objects in these galaxies. Massey [4] and Massey and Olsen [9] were the first to perform such follow-up surveys, confirming over $\sim 90\%$ of their optically-selected RSG candidates. These pioneering works were followed by other spectroscopic studies confirming photometric candidates in the Magellanic Clouds [100,101], M31 [102] and M33 [103], as well as multiple studies on dwarf irregular galaxies: WLM, NGC 3109, NGC 6822, Sextans A, IC 1613, Pegasus, Phoenix, and IC 10 [23,24,35,104–106]).

In the last 5 years or so, entire populations of RSGs in many Local Group galaxies have been identified and revised by improving the photometric selection criteria: Yang et al. [12] identified 1405 RSGs in the SMC, while Yang et al. [107] refined the catalog to 1239 RSGs, estimating the total number to be ~ 1800 . Yang et al. [108] improved the catalog cleaning and completeness, identifying 2121 RSGs. In the LMC, Yang et al. [13] found 2974 RSGs. Antoniadis et al. [91] refined the sample to 2219 RSGs. Ren et al. [109] reported 4823 and 2138 RSGs in the LMC and SMC, respectively. The latter study also identified RSGs in another 10 low-mass galaxies of the Local Group: WLM, IC 10, NGC 147, NGC 185, IC 1613, Leo A, Sextans B, Sextans A, NGC 6822, and Pegasus Dwarf. Yang et al. [13] identified ~ 300 RSG in NGC 6822 and compared the results of different selection methods. Antoniadis et al. [110] have identified 82 more RSGs in NGC 6822 from the JWST photometry of Nally et al. [111]. Boyer et al. [28] used JWST photometry to separate RSGs from thermally-pulsing AGB stars in WLM. In M31 and M33, Massey et al. [112] found 6412 RSGs in M31 and 2858 RSGs based on a near-IR photometric survey. Ren et al. [113] independently identified 5498 RSGs in M31 and 3055 RSGs in M33 using the same method, finding the estimated RSG populations for the two galaxies to agree within 10–15%.

5. RSGs Beyond the Local Group

Beyond the Local Group, several works have measured the parameters and metallicities of RSGs by obtaining *J*-band spectroscopy of targets in the Sculptor Group, e.g., NGC 300 and NGC 55 [114,115]. The ASSESS project obtained low-resolution optical spectra of RSG candidates, producing the largest catalog of RSGs at low *Z* beyond the Local Group (127 RSGs, analyzed by [29]) in NGC 55, NGC 247, NGC 253, NGC 300, NGC 1313, M83, and NGC 7793 [24,35]. This sample includes two spectroscopically confirmed RSGs beyond 4 Mpc, in M83 and NGC 1313. These are the most distant RSGs currently confirmed. Photometric RSG candidates in M83 have been identified with mid-IR colors by Williams et al. [116]. Beyond that, super star clusters dominated by RSGs have been used as abundance probes [117] in M83 [118] and NGC 4038 in the Antennae [119].

Chun et al. [120] used near-IR photometry to identify RSGs in NGC 4449, NGC 5055 (M63), and NGC 5457 (M101), which extend from 4 to 9 Mpc. However, this study took place before the near-IR criteria to remove AGB stars [12] and before *Gaia* DR2; therefore, they could not perform foreground cleaning. The machine-learning algorithm of Maravelias et al. [34] has identified over 120,000 robust candidate RSGs in nearby galaxies extending out to 5 Mpc, including over 80,000 candidates in M31, 25,000 in M33, ~ 7000 in NGC 6822, 2300 in IC 1613, and over 600 in NGC 2403 and in IC 10 [41]. Most of these are expected to be true RSGs, given the high recovery rate of the machine-learning algorithm for this class.

6. Insights from Extragalactic RSGs

Increased samples of extragalactic RSG with accurately measured parameters (T_{eff} , L , R) have greatly impacted our understanding of their physical properties and evolution. For example, the dependence of T_{eff} and the Hayashi limit on metallicity [100,106,121] resulted from the spectroscopic follow-up of RSGs in the Magellanic Clouds. Davies et al. [122] also found that effective temperatures of RSGs in the Magellanic Clouds derived from TiO bands were lower than those determined from SED fitting, because molecular bands are formed in the cooler, outer layers of the extended atmospheres of RSGs. Davies and Plez [123] further found that high mass-loss rates increase the strength of the TiO absorption bands, and that fluctuations in the wind can cause changes in spectral type. It remains unclear whether or not the extreme spectroscopic variability of Levesque–Massey variables [124,125], found primarily in low metallicity galaxies, is also caused by this mechanism. Disentangling the effects of metallicity, episodic mass loss, and T_{eff} requires improved, 3D, atmospheric models as the approximations made in the current ones cannot reproduce the complex atmospheres. Currently, this issue can be tackled with *J*-band spectroscopy and the modeling of atomic lines, e.g., [114,126,127], which yield both the metallicity and T_{eff} .

Extragalactic RSGs were also key to determining that RSG mass-loss rates are lower, e.g., [91,110] than previously considered and implemented in evolutionary models (cf. [128,129]), that the mass-loss rate relation with luminosity has a ‘kink’ around $\log L/L_{\odot} \sim 4.5$ [108,130], and that a significant fraction have dusty ejecta [29,110]. The chapter by van Loon in this Special Issue further discusses these results and their implications. Furthermore, extragalactic RSGs enabled the construction of luminosity functions, e.g., in M31 and M33, see [131,132], to directly test evolutionary models and, in particular, the position of the SN progenitors; see, e.g., [128,129]. They also determined an upper limit of $\log L/L_{\odot} \sim 5.4$, which represents the upper limit of RSG progenitors of type IIP supernovae. Finally, extragalactic RSGs can be used to constrain the various physical processes taking place, such as the driving mechanism of the winds, episodic mass loss, and the extreme phenomena observed at high luminosities, as well as the binary fraction of RSGs. The following subsections describe some of these in detail.

6.1. The Humphreys–Davidson Limit for RSGs

Improved distances to nearby galaxies combined with high-quality photometric data demand a reassessment of the Humphreys–Davidson limit [1], which was originally reported to be at $\log L/L_{\odot} = 5.8 \pm 0.1$. This value is supported by more recent studies reporting high luminosity RSGs in M31 and M33, e.g., [41,133]; these sources deserve follow-up. However, Davies et al. [134] found the upper luminosity limit of RSGs in both the Large and Small Magellanic Clouds to be $\log L/L_{\odot} \sim 5.5$. McDonald et al. [135] determined an upper luminosity limit of $\log L/L_{\odot} \sim 5.53 \pm 0.03$ for RSGs in M31, finding that many sources with higher luminosity estimates turned out to be foreground stars, or were resolved as binaries or clusters. These works therefore hint at a lower, metallicity-independent value for the HD limit in the regime of RSGs. Repeating this exercise in more galaxies will help confirm this result. Martin and Humphreys [136] identified two RSGs in the LMC that are near the higher value limit: WOH G64 and IRAS 05346-6949. However, WOH G64 has extended circumstellar material that was resolved by Ohnaka et al. [137], who also estimated a more accurate luminosity for the star, by taking into account the CSM. This value was 0.3 dex lower than the original estimation (although differences in the modeling assumptions of the dust may affect the luminosity; see, e.g., [130]). By analogy, IRAS 05346-6949 and other RSGs with $\log L/L_{\odot} \sim 5.8$ may also be revised to lower luminosities once their CSM is resolved. Munoz-Sanchez et al. [88] pointed out that Var A and other extended sources may be overestimated by 0.3 dex similarly to WOH G64, which would indeed bring the HD limit for RSGs down to $\log L/L_{\odot} \sim 5.5$.

6.2. Extreme RSGs

Extreme RSGs are defined as RSGs that are extreme in terms of both luminosity and size, pushing the limits of hydrostatic stability of the star. The evolution of these RSGs remains unclear, given the uncertainties in the mass-loss relations used by stellar evolution models in both the hot star phase and the RSG phase (see, e.g., [91,138]), the amount of stripping predicted for various mass-loss rate relations [129], the effect of binary interactions for RSGs with companions, and that of episodic mass loss, which is not yet incorporated in evolutionary models. In depth studies of individual extreme RSGs offer great insight into these rare objects (e.g., see VY CMa and NML Cyg, mentioned above). Such studies have been recently extended to extragalactic RSGs, such as WOH G64 [139] in the LMC, which have the benefit of accurate distances and therefore accurate luminosities.

WOH G64 is unique in that it has offered us the opportunity to observe post-RSG evolution in real time. It was one of the most luminous ($\log(L/L_{\odot}) = 5.45$ dex [140]) and highly mass-losing RSG in the LMC ($\dot{M} > 10^{-4} M_{\odot} \text{ yr}^{-1}$ [91,141]) until its transition to a YHG in 2014, in a symbiotic B[e] binary, discovered by Munoz-Sanchez et al. [139]. It is also the first extragalactic star to be resolved with interferometry (GRAVITY on VLTI [137]). The nature of its transition, which led to the ejection of the outer envelope of the star, remains unclear. The prevailing scenarios at the moment are (a) a pre-supernova superwind phase

caused strong pulsations that ejected the envelope, (b) grazing envelope interactions in the binary disrupted the outer envelope, and (c) WOH G64 was always a YHG, but appeared as as RSG after a high mass-loss event that created a cool pseudo-atmosphere, as in the case of Var A in M33 [142].

6.3. Dimming Events and Other Photometric Variability

The semi-regular or irregular photometric variability of RSGs is due to a combination of factors, such as radial pulsations, the effects of convection at the surface of the star, such as shocks, hot spots, and cell turnover, see, e.g., [143], and in some cases, binarity and mass loss. Photometric time series of extragalactic RSGs revealed the period–luminosity relation for RSGs [46,48,144]. Furthermore, the long secondary periods (LSPs) observed in many RSGs were proposed as the effect of a binary companion [145].

Over the past 5 years, reports of dimming events in a handful of RSGs are offering great insight into the frequency and characteristics of episodic mass loss. The luminous RSG in the LMC, [W60] B90 ($\log L/L_{\odot} = 5.32$ dex [101]) was found to exhibit three dimming events with $\Delta V \sim 1$ mag [88] (see Figure 5), similar in depth to the Great Dimming of Betelgeuse $\Delta V \sim 1.1$ mag. However, these had a recurrence period of 11.8 years and a rise time of ~ 400 days vs. ~ 200 days for Betelgeuse. Dimming events with a similar depth of $\Delta V \sim 1$ mag and rise time of ~ 400 days were also reported in RW Cep [82] and μ Cep (a minimum, in this case). Figure 5 compares the dimming events in the four stars mentioned above. The light curve rise time was found to correlate with the radius of the star, implying that smaller RSGs recover faster from dimming events, while larger RSGs take longer, which is likely related to the time needed for the atmosphere to readjust after a large convective cell rises to the surface and releases material. A calibration of this relation would make it a powerful distance indicator for RSGs, in particular those in the Milky Way, as this method is not affected by extinction. VY CMa has also exhibited a dimming event of $\Delta V \sim 3$ mag [146], with a rise time of ~ 500 days, in agreement with its larger radius. Another extreme dimming event (>2 mag in F814W) was reported by Jencson et al. [147] in a $\log L/L_{\odot} \sim 5.2$ RSG in M51, although it was not constrained well in time.

Extending such studies to large samples of extragalactic RSGs will help determine the frequency and characteristics of dimming events as a function of luminosity.

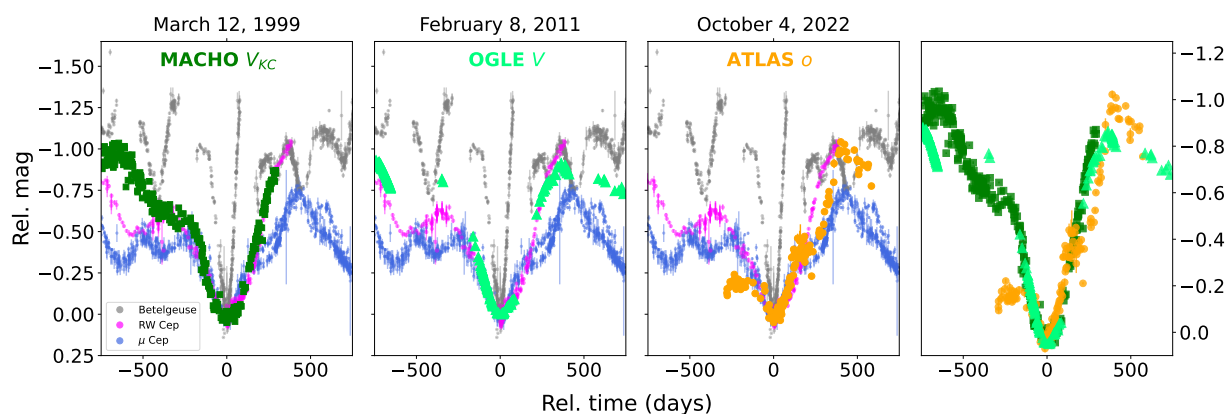


Figure 5. The three dimming events in [W60] B90 (dark and bright green, and orange points, respectively [88]). The first three panels compare the dimming events of [W60] B90 with the Great Dimming of Betelgeuse (gray), the dimming of RW Cep (magenta), and a minimum from μ Cep (blue) in the V-band from AAVSO. The right panel overplots the three dimming event light curves of [W60] B90. The minimum of each dataset was used as the zero-point reference for each panel. (reproduced from [88]).

6.4. RSGs in Binary Systems

The last few years have seen a renewed interest in RSGs in binary systems, following the finding that binary interactions dominate the evolution of massive stars and that over

70% of all massive stars are expected to interact [148]. Several studies have been undertaken, resulting in great leaps in our understanding of binary RSGs. Neugent et al. [149] list the 11 Galactic binary RSGs known before 2019, all with spectroscopically confirmed B-type companions, as these have the largest contrast and are therefore the easiest to detect. RSGs in binary systems are expected to be in orbits with periods longer than 1000 days, so that the RSG does not fill its Roche lobe [148,150].

The survey of cool supergiants in the Magellanic Clouds by González-Fernández et al. [151] found about a dozen binary RSG candidates. It was followed by more systematic surveys for binary RSGs. Neugent et al. [149] used photometric color-criteria to select UV-bright RSGs as candidate binaries and confirmed 87 binary RSGs spectroscopically, 63 in M31 and M33, and the rest in the Magellanic Clouds [152]. Neugent et al. [149] increased the LMC sample by 38 binaries, while Neugent et al. [150] determined the binary frequency in the LMC to be $\sim 20\%$. Neugent [153] found a higher binary frequency of $\sim 30\%$ in M31, and a clear metallicity-dependence in M33, with the frequency dropping from $\sim 40\%$ in the center to 16% in the outer regions. Patrick et al. [154] used photometry from the Ultraviolet Imaging Telescope (UVIT) on board *AstroSat* to determine the intrinsic binarity fraction of RSGs in the SMC to be $\sim 19\%$, while Patrick et al. [155] confirmed 16 B-type companions of RSGs with ultra-violet spectroscopy.

Two recent studies have presented evidence for a low-mass companion to Betelgeuse to explain its long secondary period [145,156]. The mass of the companion is inferred to be $\lesssim 1 - 2 M_{\odot}$, which, if conatal, implies a pre-main sequence star. This opens a new parameter space for low-mass RSG companions, which at the moment elude detection. Finally, there have been searches for binaries with exotic companions among extragalactic RSGs, such as neutron stars that could appear as Thorne–Żytkow objects. Levesque et al. [157] reported the first such candidate in the SMC, while DeMarchi et al. [158] suggest the detection of such exotic binaries with gravitational waves and multi-messenger observations.

6.5. Red Stragglers

Red stragglers are RSGs in a cluster that are more luminous and massive than expected from single-star evolution. They are thought to be stars rejuvenated by mass accretion and mergers in binary systems, and are therefore descendants or evolved products of blue stragglers. Britavskiy et al. [159] were the first to identify such stars and to coin the term ‘red stragglers’. They were found as luminous RSG outliers in two open clusters in the LMC and had a large age spread. Beasor et al. [160] arrived at the same conclusions by studying two open clusters in the Milky Way and two in the LMC. Patrick et al. [161] found a red straggler fraction of 50% among RSGs in the SMC. Wang et al. [162], however, found that binary effects alone cannot account for the luminosity spread in open clusters.

7. Future Outlook

The recent advancements outlined above, including the improvement of selection criteria, flagging foreground sources and contaminants, and the development of machine-learning algorithms for identifying RSGs, along with spectroscopic follow-up efforts and the expansion of archival data, have resulted in constraints that demand accurate modeling. Full 3D models of stellar atmospheres, e.g., CO5BOLD [163,164], are needed to resolve the inconsistencies encountered with the 1D MARCS models [51], such as the T_{eff} measured using different parts of RSG spectra. They will also be able to make predictions about the variability in RSG spectra and light curves, including dimming events. Furthermore, improved evolutionary models for single stars, including the new mass-loss rate prescriptions and episodic mass loss are needed for accurately placing RSGs on the Hertzsprung–Russell diagram and for predicting the location of SN progenitors. The next step would be to incorporate accurate single-star physics into binary evolution modeling, e.g., see POSYDON [165,166].

Observationally, the spectroscopic confirmation of RSGs at 1 Mpc or beyond remains ‘expensive’ as it requires significant observing time on 8–10 m class telescopes. The same

holds for highly extinguished RSGs in the Milky Way, which require near-IR spectroscopy. The multi-object capabilities of both optical and near-IR spectrographs accelerate the rate at which spectra can be collected; however, given that the fields of view of multi-object spectrographs are typically smaller than the sizes of most nearby galaxies, multiple pointings are required. The most distant RSGs to be confirmed spectroscopically are at ~ 4.5 Mpc (in NGC 1313 and M83 [24]). Besides securing telescope time, current observational challenges facing the confirmation of an RSG candidate include removing contaminants, which can be mitigated using astrometric data from *Gaia*, the position on near-IR CMD, and time-series photometric data, when available.

The future is promising, with JWST and other new missions that will characterize full populations of RSGs in nearby galaxies; interferometry, which will resolve a larger number of nearby RSGs; the ELT, which will make possible very high-resolution and high-sensitivity observations; and LSST, which will provide unprecedented time-series photometry and reveal the variability properties of RSGs in galaxies beyond 10 Mpc. Finally, machine-learning algorithms and AI are expected to exploit the exponential increase of astronomical data from existing and future large-scale surveys and significantly advance our knowledge of the final evolutionary stages of massive stars in the next decade.

Funding: This research received no external funding.

Data Availability Statement: No new data were created or analyzed in this study. Data sharing is not applicable to this article.

Conflicts of Interest: The author declares no conflicts of interest.

Abbreviations

The following abbreviations are used in this manuscript:

2MASS	Two-Micron All Sky Survey
AAVSO	American Association of Variable Star Observers
AI	Artificial Intelligence
ALMA	Atacama Large Millimeter/submillimeter Array
CHARA	Center for High Angular Resolution Astronomy
CMD	Color–Magnitude Diagram
ELT	Extremely Large Telescope
HST	Hubble Space Telescope
IR	Infrared
JWST	James Webb Space Telescope
LMC	Large Magellanic Cloud
LSST	Legacy Survey of Space and Time
MARCS	Model Atmospheres with a Radiative and Convective Scheme
MERLIN	Multi-Element Radio Linked Interferometer Network
MMT	Multiple Mirror Telescope
OGLE	Optical Gravitational Lensing Experiment
POSDON	POpulation SYNthesis with Detailed binary-evolution simulatiONs
RSG	Red Supergiant
SED	Spectral Energy Distribution
SMC	Small Magellanic Cloud
WISE	Wide-field Infrared Survey Explorer
VLA	Very Large Array
VLT	Very Large Telescope
YHG	Yellow Hypergiant
ZAMS	Zero-Age Main Sequence

References

1. Humphreys, R.M.; Davidson, K. Studies of luminous stars in nearby galaxies. III. Comments on the evolution of the most massive stars in the Milky Way and the Large Magellanic Cloud. *ApJ* **1979**, *232*, 409–420. <https://doi.org/10.1086/157301>.
2. Humphreys, R.W. M Supergiants in the Perseus Arm. *ApJ* **1970**, *160*, 1149. <https://doi.org/10.1086/150502>.

3. Humphreys, R.M. Studies of luminous stars in nearby galaxies. II. M supergiants in the Large Magellanic Cloud. *ApJS* **1979**, *39*, 389–403. <https://doi.org/10.1086/190578>.
4. Massey, P. Evolved Massive Stars in the Local Group. I. Identification of Red Supergiants in NGC 6822, M31, and M33. *ApJ* **1998**, *501*, 153–174. <https://doi.org/10.1086/305818>.
5. Massey, P. A UBV_r CCD Survey of the Magellanic Clouds. *ApJS* **2002**, *141*, 81–122, [arXiv:astro-ph/astro-ph/0110531]. <https://doi.org/10.1086/338286>.
6. Massey, P.; McNeill, R.T.; Olsen, K.A.G.; Hodge, P.W.; Blaha, C.; Jacoby, G.H.; Smith, R.C.; Strong, S.B. A Survey of Local Group Galaxies Currently Forming Stars. III. A Search for Luminous Blue Variables and Other H α Emission-Line Stars. *AJ* **2007**, *134*, 2474–2503, [arXiv:astro-ph/0709.1267]. <https://doi.org/10.1086/523658>.
7. Brunish, W.M.; Gallagher, J.S.; Truran, J.W. Blue-to-red ratios as tests for theoretical models of massive stars. *AJ* **1986**, *91*, 598–601. <https://doi.org/10.1086/114042>.
8. Rayner, J.T.; Cushing, M.C.; Vacca, W.D. The Infrared Telescope Facility (IRTF) Spectral Library: Cool Stars. *ApJS* **2009**, *185*, 289–432, [arXiv:astro-ph.SR/0909.0818]. <https://doi.org/10.1088/0067-0049/185/2/289>.
9. Massey, P.; Olsen, K.A.G. The Evolution of Massive Stars. I. Red Supergiants in the Magellanic Clouds. *AJ* **2003**, *126*, 2867–2886, [arXiv:astro-ph/astro-ph/0309272]. <https://doi.org/10.1086/379558>.
10. Negueruela, I.; Schurch, M.P.E. A search for counterparts to massive X-ray binaries using photometric catalogues. *A&A* **2007**, *461*, 631–639, [arXiv:astro-ph/astro-ph/0610006]. <https://doi.org/10.1051/0004-6361/20066054>.
11. Messineo, M.; Zhu, Q.; Menten, K.M.; Ivanov, V.D.; Figer, D.F.; Kudritzki, R.P.; Chen, C.H.R. Discovery of an Extraordinary Number of Red Supergiants in the Inner Galaxy. *ApJ* **2016**, *822*, L5. <https://doi.org/10.3847/2041-8205/822/1/L5>.
12. Yang, M.; Bonanos, A.Z.; Jiang, B.W.; Gao, J.; Gavras, P.; Maravelias, G.; Ren, Y.; Wang, S.; Xue, M.Y.; Tramper, F.; et al. Evolved massive stars at low-metallicity. I. A source catalog for the Small Magellanic Cloud. *A&A* **2019**, *629*, A91, [arXiv:astro-ph.SR/1907.06717]. <https://doi.org/10.1051/0004-6361/201935916>.
13. Yang, M.; Bonanos, A.Z.; Jiang, B.; Lam, M.I.; Gao, J.; Gavras, P.; Maravelias, G.; Wang, S.; Chen, X.D.; Tramper, F.; et al. Evolved massive stars at low-metallicity. IV. Using the 1.6 μ m H-bump to identify red supergiant stars: Case study of NGC 6822. *A&A* **2021**, *647*, A167, [arXiv:astro-ph.SR/2101.08689]. <https://doi.org/10.1051/0004-6361/202039596>.
14. Li, Z.w.; Yang, M.; Jiang, B.; Ren, Y. A New Approach to Identifying Red Supergiant Stars in Metal-poor Galaxies: A Case Study of NGC 6822. *ApJ* **2025**, *979*, 208, [arXiv:astro-ph.GA/2412.15763]. <https://doi.org/10.3847/1538-4357/ada1d4>.
15. Yang, M.; Zhang, B.; Jiang, B.; Gao, J.; Ren, Y.; Wang, S.; Lam, M.I.; Tian, H.; Luo, C.; Chen, B.; et al. Evolved Massive Stars at Low Metallicity. VII. The Lower Mass Limit of the Red Supergiant Population in the Large Magellanic Cloud. *ApJ* **2024**, *965*, 106, [arXiv:astro-ph.SR/2401.15832]. <https://doi.org/10.3847/1538-4357/ad28c4>.
16. Meixner, M.; Gordon, K.D.; Indebetouw, R.; et al. Spitzer Survey of the Large Magellanic Cloud: Surveying the Agents of a Galaxy's Evolution (SAGE). I. Overview and Initial Results. *AJ* **2006**, *132*, 2268–2288, [arXiv:astro-ph/astro-ph/0606356]. <https://doi.org/10.1086/508185>.
17. Gordon, K.D.; Meixner, M.; Meade, M.R.; et al. Surveying the Agents of Galaxy Evolution in the Tidally Stripped, Low Metallicity Small Magellanic Cloud (SAGE-SMC). I. Overview. *AJ* **2011**, *142*, 102, [arXiv:astro-ph.CO/1107.4313]. <https://doi.org/10.1088/0004-6256/142/4/102>.
18. Bonanos, A.Z.; Massa, D.L.; Sewilo, M.; et al. Spitzer SAGE Infrared Photometry of Massive Stars in the Large Magellanic Cloud. *AJ* **2009**, *138*, 1003–1021, [arXiv:astro-ph.SR/0905.1328]. <https://doi.org/10.1088/0004-6256/138/4/1003>.
19. Bonanos, A.Z.; Lennon, D.J.; Köhlinger, F.; et al. Spitzer SAGE-SMC Infrared Photometry of Massive Stars in the Small Magellanic Cloud. *AJ* **2010**, *140*, 416–429, [arXiv:astro-ph.SR/1004.0949]. <https://doi.org/10.1088/0004-6256/140/2/416>.
20. Verhoelst, T.; van der Zypen, N.; Hony, S.; Decin, L.; Cami, J.; Eriksson, K. The dust condensation sequence in red supergiant stars. *A&A* **2009**, *498*, 127–138, [arXiv:astro-ph.SR/0901.1262]. <https://doi.org/10.1051/0004-6361/20079063>.
21. Waters, L.B.F.M. Circumstellar Dust in Massive Stars. In Proceedings of the Hot and Cool: Bridging Gaps in Massive Star Evolution; Leitherer, C.; Bennett, P.D.; Morris, P.W.; Van Loon, J.T., Eds., 2010, Vol. 425, *Astronomical Society of the Pacific Conference Series*, p. 267.
22. Messineo, M.; Menten, K.M.; Churchwell, E.; Habing, H. Near- and mid-infrared colors of evolved stars in the Galactic plane. The Q1 and Q2 parameters. *A&A* **2012**, *537*, A10, [arXiv:astro-ph.GA/1110.6843]. <https://doi.org/10.1051/0004-6361/201117772>.
23. Britavskiy, N.E.; Bonanos, A.Z.; Mehner, A.; et al. Identification of dusty massive stars in star-forming dwarf irregular galaxies in the Local Group with mid-IR photometry. *A&A* **2015**, *584*, A33, [arXiv:astro-ph.SR/1510.01340]. <https://doi.org/10.1051/0004-6361/201526393>.
24. Bonanos, A.Z.; Tramper, F.; de Wit, S.; Christodoulou, E.; Muñoz Sanchez, G.; Antoniadis, K.; Athanasiou, S.; Maravelias, G.; Yang, M.; Zapartas, E. Investigating episodic mass loss in evolved massive stars. I. Spectroscopy of dusty massive stars in ten southern galaxies. *A&A* **2024**, *686*, A77, [arXiv:astro-ph.GA/2312.04626]. <https://doi.org/10.1051/0004-6361/202348527>.
25. Lee, J.C.; Sandstrom, K.M.; Leroy, A.K.; Thilker, D.A.; Schinnerer, E.; Rosolowsky, E.; Larson, K.L.; Egorov, O.V.; Williams, T.G.; Schmidt, J.; et al. The PHANGS-JWST Treasury Survey: Star Formation, Feedback, and Dust Physics at High Angular Resolution in Nearby Galaxies. *ApJ* **2023**, *944*, L17, [arXiv:astro-ph.GA/2212.02667]. <https://doi.org/10.3847/2041-8213/acaade>.
26. Williams, T.G.; Lee, J.C.; Larson, K.L.; Leroy, A.K.; Sandstrom, K.; Schinnerer, E.; Thilker, D.A.; Belfiore, F.; Egorov, O.V.; Rosolowsky, E.; et al. PHANGS-JWST: Data-processing Pipeline and First Full Public Data Release. *ApJS* **2024**, *273*, 13, [arXiv:astro-ph.GA/2401.15142]. <https://doi.org/10.3847/1538-4365/ad4be5>.

27. Levesque, E.M. Red Supergiants in the JWST Era. I. Near-IR Photometric Diagnostics. *ApJ* **2018**, *867*, 155, [arXiv:astro-ph.SR/1810.04187]. <https://doi.org/10.3847/1538-4357/aae776>.
28. Boyer, M.L.; Pastorelli, G.; Girardi, L.; Marigo, P.; Dolphin, A.E.; McQuinn, K.B.W.; Newman, M.J.B.; Savino, A.; Weisz, D.R.; Williams, B.F.; et al. The JWST Resolved Stellar Populations Early Release Science Program. VI. Identifying Evolved Stars in Nearby Galaxies. *ApJ* **2024**, *973*, 120, [arXiv:astro-ph.GA/2401.14889]. <https://doi.org/10.3847/1538-4357/ad6449>.
29. de Wit, S.; Bonanos, A.Z.; Antoniadis, K.; Zapartas, E.; Ruiz, A.; Britavskiy, N.; Christodoulou, E.; De, K.; Maravelias, G.; Muñoz-Sánchez, G.; et al. Investigating episodic mass loss in evolved massive stars: II. Physical properties of red supergiants at subsolar metallicity. *A&A* **2024**, *689*, A46, [arXiv:astro-ph.SR/2402.12442]. <https://doi.org/10.1051/0004-6361/202449607>.
30. Gaia Collaboration.; Prusti, T.; de Bruijne, J.H.J.; Brown, A.G.A.; Vallenari, A.; Babusiaux, C.; Bailer-Jones, C.A.L.; Bastian, U.; Biermann, M.; Evans, D.W.; et al. The Gaia mission. *A&A* **2016**, *595*, A1, [arXiv:astro-ph.IM/1609.04153]. <https://doi.org/10.1051/0004-6361/201629272>.
31. Gaia Collaboration.; Brown, A.G.A.; Vallenari, A.; Prusti, T.; de Bruijne, J.H.J.; Babusiaux, C.; Bailer-Jones, C.A.L.; Biermann, M.; Evans, D.W.; Eyer, L.; et al. Gaia Data Release 2. Summary of the contents and survey properties. *A&A* **2018**, *616*, A1, [arXiv:astro-ph.GA/1804.09365]. <https://doi.org/10.1051/0004-6361/201833051>.
32. Gaia Collaboration.; Vallenari, A.; Brown, A.G.A.; Prusti, T.; de Bruijne, J.H.J.; Arenou, F.; Babusiaux, C.; Biermann, M.; Creevey, O.L.; Ducourant, C.; et al. Gaia Data Release 3. Summary of the content and survey properties. *A&A* **2023**, *674*, A1, [arXiv:astro-ph.GA/2208.00211]. <https://doi.org/10.1051/0004-6361/202243940>.
33. Aadland, E.; Massey, P.; Neugent, K.F.; Drout, M.R. Shedding Light on the Isolation of Luminous Blue Variables. *AJ* **2018**, *156*, 294, [arXiv:astro-ph.SR/1810.11169]. <https://doi.org/10.3847/1538-3881/aaeb96>.
34. Maravelias, G.; Bonanos, A.Z.; Tramper, F.; de Wit, S.; Yang, M.; Bonfini, P. A machine-learning photometric classifier for massive stars in nearby galaxies. I. The method. *A&A* **2022**, *666*, A122, [arXiv:astro-ph.SR/2203.08125]. <https://doi.org/10.1051/0004-6361/202141397>.
35. de Wit, S.; Muñoz-Sánchez, G.; Maravelias, G.; Bonanos, A.Z.; Antoniadis, K.; García-Álvarez, D.; Britavskiy, N.; Ruiz, A.; Philippopoulos, A. Investigating episodic mass loss in evolved massive stars: III. Spectroscopy of dusty massive stars in three northern galaxies. *A&A* **2025**, pp. (arXiv:2505.01498), in press, [arXiv:astro-ph.SR/2505.01498]. <https://doi.org/10.48550/arXiv.2505.01498>.
36. Dorda, R.; González-Fernández, C.; Negueruela, I. Characterisation of red supergiants in the Gaia spectral range. *A&A* **2016**, *595*, A105, [arXiv:astro-ph.SR/1609.04063]. <https://doi.org/10.1051/0004-6361/201628422>.
37. Messineo, M. Identification of late-type Class I stars using Gaia DR3 Apsis parameters. *A&A* **2023**, *671*, A148, [arXiv:astro-ph.SR/2301.07415]. <https://doi.org/10.1051/0004-6361/202245587>.
38. Zhang, Z.; Jiang, B.; Ren, Y.; Zhao, H.; Yang, M. Searching for Galactic Red Supergiants with Gaia RVS Spectra. *arXiv e-prints* **2024**, p. arXiv:2412.17393, [arXiv:astro-ph.SR/2412.17393]. <https://doi.org/10.48550/arXiv.2412.17393>.
39. Dorn-Wallenstein, T.Z.; Neugent, K.F.; Levesque, E.M. Physical Properties of 5000 Cool Large Magellanic Cloud Supergiants with Gaia XP Spectra: A Detailed Portrait of the Upper H-R Diagram Hints at Missing Supernova Progenitors. *ApJ* **2023**, *959*, 102, [arXiv:astro-ph.SR/2310.16088]. <https://doi.org/10.3847/1538-4357/ad0725>.
40. Dorn-Wallenstein, T.Z.; Davenport, J.R.A.; Huppenkothen, D.; Levesque, E.M. Photometric Classifications of Evolved Massive Stars: Preparing for the Era of Webb and Roman with Machine Learning. *ApJ* **2021**, *913*, 32, [arXiv:astro-ph.SR/2102.02829]. <https://doi.org/10.3847/1538-4357/abff1f2>.
41. Maravelias, G.; Bonanos, A.Z.; Antoniadis, K.; Muñoz-Sánchez, G.; Christodoulou, E.; de Wit, S.; Zapartas, E.; Kovlakas, K.; Tramper, F.; Bonfini, P.; et al. A machine-learning photometric classifier for massive stars in nearby galaxies II. The catalog. *A&A, subm.* **2025**, p. (arXiv:2504.01232), [arXiv:astro-ph.GA/2504.01232].
42. Kiss, L.L.; Szabó, G.M.; Bedding, T.R. Variability in red supergiant stars: pulsations, long secondary periods and convection noise. *MNRAS* **2006**, *372*, 1721–1734, [arXiv:astro-ph/astro-ph/0608438]. <https://doi.org/10.1111/j.1365-2966.2006.10973.x>.
43. Szczygieł, D.M.; Stanek, K.Z.; Bonanos, A.Z.; Pojmański, G.; Pilecki, B.; Prieto, J.L. Variability of Luminous Stars in the Large Magellanic Cloud Using 10 Years of ASAS Data. *AJ* **2010**, *140*, 14–24, [arXiv:astro-ph.SR/1001.3410]. <https://doi.org/10.1088/0004-6256/140/1/14>.
44. Yang, M.; Bonanos, A.Z.; Jiang, B.W.; Gao, J.; Xue, M.Y.; Wang, S.; Lam, M.I.; Spetsieri, Z.T.; Ren, Y.; Gavras, P. Red supergiant stars in the Large Magellanic Cloud. II. Infrared properties and mid-infrared variability. *A&A* **2018**, *616*, A175, [arXiv:astro-ph.SR/1805.03290]. <https://doi.org/10.1051/0004-6361/201832833>.
45. Soraisam, M.D.; Bildsten, L.; Drout, M.R.; Bauer, E.B.; Gilfanov, M.; Kupfer, T.; Laher, R.R.; Masci, F.; Prince, T.A.; Kulkarni, S.R.; et al. Variability of Red Supergiants in M31 from the Palomar Transient Factory. *ApJ* **2018**, *859*, 73, [arXiv:astro-ph.SR/1803.09934]. <https://doi.org/10.3847/1538-4357/aabc59>.
46. Yang, M.; Jiang, B.W. The Period-Luminosity Relation of Red Supergiant Stars in the Small Magellanic Cloud. *ApJ* **2012**, *754*, 35, [arXiv:astro-ph.SR/1205.1275]. <https://doi.org/10.1088/0004-637X/754/1/35>.
47. Ren, Y.; Jiang, B.W.; Yang, M.; Gao, J. The Period-Luminosity Relations of Red Supergiants in M33 and M31. *ApJS* **2019**, *241*, 35, [arXiv:astro-ph.SR/1902.07597]. <https://doi.org/10.3847/1538-4365/ab0825>.
48. Chatys, F.W.; Bedding, T.R.; Murphy, S.J.; Kiss, L.L.; Dobie, D.; Grindlay, J.E. The period-luminosity relation of red supergiants with Gaia DR2. *MNRAS* **2019**, *487*, 4832–4846, [arXiv:astro-ph.SR/1906.03879]. <https://doi.org/10.1093/mnras/stz1584>.

49. Ren, Y.; Jiang, B.W. On the Granulation and Irregular Variation of Red Supergiants. *ApJ* **2020**, *898*, 24, [arXiv:astro-ph.SR/2006.06605]. <https://doi.org/10.3847/1538-4357/ab9c17>.
50. Messineo, M.; Figer, D.F.; Kudritzki, R.P.; Zhu, Q.; Menten, K.M.; Ivanov, V.D.; Chen, C.H.R. New Infrared Spectral Indices of Luminous Cold Stars: From Early K to M Types. *AJ* **2021**, *162*, 187, [arXiv:astro-ph.SR/2107.03707]. <https://doi.org/10.3847/1538-3881/ac116b>.
51. Gustafsson, B.; Edvardsson, B.; Eriksson, K.; Jørgensen, U.G.; Nordlund, Å.; Plez, B. A grid of MARCS model atmospheres for late-type stars. I. Methods and general properties. *A&A* **2008**, *486*, 951–970, [arXiv:astro-ph/0805.0554]. <https://doi.org/10.1051/0004-6361:200809724>.
52. Bergemann, M.; Lind, K.; Collet, R.; et al. Non-LTE line formation of Fe in late-type stars - I. Standard stars with 1D and <3D> model atmospheres. *MNRAS* **2012**, *427*, 27–49, [arXiv:astro-ph.SR/1207.2455]. <https://doi.org/10.1111/j.1365-2966.2012.21687.x>.
53. Bergemann, M.; Kudritzki, R.P.; Würl, M.; et al. Red Supergiant Stars as Cosmic Abundance Probes. II. NLTE Effects in J-band Silicon Lines. *ApJ* **2013**, *764*, 115, [arXiv:astro-ph.SR/1212.2649]. <https://doi.org/10.1088/0004-637X/764/2/115>.
54. Bergemann, M.; Kudritzki, R.P.; Gazak, Z.; et al. Red Supergiant Stars as Cosmic Abundance Probes. III. NLTE effects in J-band Magnesium Lines. *ApJ* **2015**, *804*, 113, [arXiv:astro-ph.SR/1412.6527]. <https://doi.org/10.1088/0004-637X/804/2/113>.
55. Haubois, X.; Perrin, G.; Lacour, S.; Verhoelst, T.; Meimon, S.; Mugnier, L.; Thiébaud, E.; Berger, J.P.; Ridgway, S.T.; Monnier, J.D.; et al. Imaging the spotty surface of <ASTROBJ>Betelgeuse</ASTROBJ> in the H band. *A&A* **2009**, *508*, 923–932, [arXiv:astro-ph.SR/0910.4167]. <https://doi.org/10.1051/0004-6361/200912927>.
56. Neilson, H.R.; Lester, J.B.; Haubois, X. Weighing Betelgeuse: Measuring the Mass of α Orionis from Stellar Limb-darkening. In Proceedings of the 9th Pacific Rim Conference on Stellar Astrophysics; Qain, S.; Leung, K.; Zhu, L.; Kwok, S., Eds., 2011, Vol. 451, *Astronomical Society of the Pacific Conference Series*, p. 117, [arXiv:astro-ph.SR/1109.4562]. <https://doi.org/10.48550/arXiv.1109.4562>.
57. Cannon, E.; Montargès, M.; de Koter, A.; Matter, A.; Sanchez-Bermudez, J.; Norris, R.; Paladini, C.; Decin, L.; Sana, H.; Sundqvist, J.O.; et al. The dusty circumstellar environment of Betelgeuse during the Great Dimming as seen by VLTI/MATISSE. *A&A* **2023**, *675*, A46, [arXiv:astro-ph.SR/2303.08892]. <https://doi.org/10.1051/0004-6361/202243611>.
58. Joyce, M.; Leung, S.C.; Molnár, L.; Ireland, M.; Kobayashi, C.; Nomoto, K. Standing on the Shoulders of Giants: New Mass and Distance Estimates for Betelgeuse through Combined Evolutionary, Asteroseismic, and Hydrodynamic Simulations with MESA. *ApJ* **2020**, *902*, 63, [arXiv:astro-ph.SR/2006.09837]. <https://doi.org/10.3847/1538-4357/abb8db>.
59. Harper, G.M.; Brown, A.; Guinan, E.F.; O’Gorman, E.; Richards, A.M.S.; Kervella, P.; Decin, L. An Updated 2017 Astrometric Solution for Betelgeuse. *AJ* **2017**, *154*, 11, [arXiv:astro-ph.SR/1706.06020]. <https://doi.org/10.3847/1538-3881/aa6ff9>.
60. Figer, D.F.; MacKenty, J.W.; Robberto, M.; Smith, K.; Najarro, F.; Kudritzki, R.P.; Herrero, A. Discovery of an Extraordinarily Massive Cluster of Red Supergiants. *ApJ* **2006**, *643*, 1166–1179, [arXiv:astro-ph/astro-ph/0602146]. <https://doi.org/10.1086/503275>.
61. Clark, J.S.; Negueruela, I.; Davies, B.; Larionov, V.M.; Ritchie, B.W.; Figer, D.F.; Messineo, M.; Crowther, P.A.; Arkharov, A.A. A third red supergiant rich cluster in the Scutum-Crux arm. *A&A* **2009**, *498*, 109–114, [arXiv:astro-ph.GA/0903.1754]. <https://doi.org/10.1051/0004-6361/200911945>.
62. Negueruela, I.; González-Fernández, C.; Marco, A.; Clark, J.S.; Martínez-Núñez, S. Another cluster of red supergiants close to RSGC1. *A&A* **2010**, *513*, A74, [arXiv:astro-ph.GA/1002.1823]. <https://doi.org/10.1051/0004-6361/200913373>.
63. Negueruela, I.; González-Fernández, C.; Marco, A.; Clark, J.S. A massive association around the obscured open cluster RSGC3. *A&A* **2011**, *528*, A59, [arXiv:astro-ph.GA/1102.0028]. <https://doi.org/10.1051/0004-6361/201016102>.
64. Negueruela, I.; Marco, A.; González-Fernández, C.; Jiménez-Esteban, F.; Clark, J.S.; Garcia, M.; Solano, E. Red supergiants around the obscured open cluster Stephenson 2. *A&A* **2012**, *547*, A15, [arXiv:astro-ph.GA/1208.3282]. <https://doi.org/10.1051/0004-6361/201219540>.
65. Marco, A.; Negueruela, I. NGC 7419 as a template for red supergiant clusters. *A&A* **2013**, *552*, A92, [arXiv:astro-ph.SR/1302.5649]. <https://doi.org/10.1051/0004-6361/201220750>.
66. Clark, J.S.; Negueruela, I.; Crowther, P.A.; Goodwin, S.P. On the massive stellar population of the super star cluster <ASTROBJ>Westerlund 1</ASTROBJ>. *A&A* **2005**, *434*, 949–969, [arXiv:astro-ph/astro-ph/0504342]. <https://doi.org/10.1051/0004-6361:20042413>.
67. Blum, R.D.; Sellgren, K.; Depoy, D.L. Really Cool Stars at the Galactic Center. *AJ* **1996**, *112*, 1988, [arXiv:astro-ph/astro-ph/9608107]. <https://doi.org/10.1086/118157>.
68. Dorda, R.; Negueruela, I.; González-Fernández, C. The red supergiant population in the Perseus arm. *MNRAS* **2018**, *475*, 2003–2015, [arXiv:astro-ph.SR/1712.08176]. <https://doi.org/10.1093/mnras/stx3317>.
69. Humphreys, R.M. Studies of luminous stars in nearby galaxies. I. Supergiants and O stars in the Milky Way. *ApJS* **1978**, *38*, 309–350. <https://doi.org/10.1086/190559>.
70. de Burgos, A.; Simon-Díaz, S.; Lennon, D.J.; Dorda, R.; Negueruela, I.; Urbaneja, M.A.; Patrick, L.R.; Herrero, A. High-resolution spectroscopic study of massive blue and red supergiants in Perseus OB1. I. Definition of the sample, membership, and kinematics. *A&A* **2020**, *643*, A116, [arXiv:astro-ph.SR/2008.13299]. <https://doi.org/10.1051/0004-6361/202039019>.
71. Healy, S.; Horiuchi, S.; Colomer Molla, M.; Milisavljevic, D.; Tseng, J.; Bergin, F.; Weil, K.; Tanaka, M.; Otero, S. Red supergiant candidates for multimessenger monitoring of the next Galactic supernova. *MNRAS* **2024**, *529*, 3630–3650, [arXiv:astro-ph.SR/2307.08785]. <https://doi.org/10.1093/mnras/stae738>.

72. Gehrz, R. Sources of Stardust in the Galaxy. In Proceedings of the Interstellar Dust; Allamandola, L.J.; Tielens, A.G.G.M., Eds., 1989, Vol. 135, *IAU Symposium*, p. 445.
73. Zhang, L.; Chen, B.; Ren, Y.; Zhang, Z.; Gao, J.; Jiang, B. New Red Supergiant Stars in the other side of our Galaxy, 2025, [arXiv:astro-ph.GA/2502.11496].
74. Smith, N.; Humphreys, R.M.; Davidson, K.; Gehrz, R.D.; Schuster, M.T.; Krautter, J. The Asymmetric Nebula Surrounding the Extreme Red Supergiant VY Canis Majoris. *AJ* **2001**, *121*, 1111–1125. <https://doi.org/10.1086/318748>.
75. Kervella, P.; Verhoelst, T.; Ridgway, S.T.; Perrin, G.; Lacour, S.; Cami, J.; Haubois, X. The close circumstellar environment of Betelgeuse. Adaptive optics spectro-imaging in the near-IR with VLT/NACO. *A&A* **2009**, *504*, 115–125, [arXiv:astro-ph.SR/0907.1843]. <https://doi.org/10.1051/0004-6361/200912521>.
76. Montargès, M.; Cannon, E.; Lagadec, E.; de Koter, A.; Kervella, P.; Sanchez-Bermudez, J.; Paladini, C.; Cantalloube, F.; Decin, L.; Scicluna, P.; et al. A dusty veil shading Betelgeuse during its Great Dimming. *Nature* **2021**, *594*, 365–368, [arXiv:astro-ph.SR/2201.10551]. <https://doi.org/10.1038/s41586-021-03546-8>.
77. Shenoy, D.; Humphreys, R.M.; Jones, T.J.; Marengo, M.; Gehrz, R.D.; Helton, L.A.; Hoffmann, W.F.; Skemer, A.J.; Hinz, P.M. Searching for Cool Dust in the Mid-to-far Infrared: The Mass-loss Histories of the Hypergiants μ Cep, VY CMa, IRC+10420, and ρ Cas. *AJ* **2016**, *151*, 51, [arXiv:astro-ph.SR/1512.01529]. <https://doi.org/10.3847/0004-6256/151/3/51>.
78. Gordon, M.S.; Humphreys, R.M.; Jones, T.J.; Shenoy, D.; Gehrz, R.D.; Helton, L.A.; Marengo, M.; Hinz, P.M.; Hoffmann, W.F. Searching for Cool Dust. II. Infrared Imaging of The OH/IR Supergiants, NML Cyg, VX Sgr, S Per, and the Normal Red Supergiants RS Per and T Per. *AJ* **2018**, *155*, 212, [arXiv:astro-ph.SR/1708.00018]. <https://doi.org/10.3847/1538-3881/aab961>.
79. González-Torà, G.; Wittkowski, M.; Davies, B.; Plez, B. The effect of winds on atmospheric layers of red supergiants II. Modelling VLTI/GRAVITY and MATISSE observations of AH Sco, KW Sgr, V602 Car, CK Car, and V460 Car. *A&A* **2024**, *683*, A19, [arXiv:astro-ph.SR/2312.12521]. <https://doi.org/10.1051/0004-6361/202348047>.
80. Richards, A.M.S.; Impellizzeri, C.M.V.; Humphreys, E.M.; Vlahakis, C.; Vlemmings, W.; Baudry, A.; De Beck, E.; Decin, L.; Etoka, S.; Gray, M.D.; et al. ALMA sub-mm maser and dust distribution of VY Canis Majoris. *A&A* **2014**, *572*, L9, [arXiv:astro-ph.SR/1409.5497]. <https://doi.org/10.1051/0004-6361/201425024>.
81. Norris, R.P.; Baron, F.R.; Monnier, J.D.; Paladini, C.; Anderson, M.D.; Martinez, A.O.; Schaefer, G.H.; Che, X.; Chiavassa, A.; Connelley, M.S.; et al. Long Term Evolution of Surface Features on the Red Supergiant AZ Cyg. *ApJ* **2021**, *919*, 124, [arXiv:astro-ph.SR/2106.15636]. <https://doi.org/10.3847/1538-4357/ac0c7e>.
82. Anugu, N.; Baron, F.; Gies, D.R.; Lanthermann, C.; Schaefer, G.H.; Shepard, K.A.; Brummelaar, T.t.; Monnier, J.D.; Kraus, S.; Le Bouquin, J.B.; et al. The Great Dimming of the Hypergiant Star RW Cephei: CHARA Array Images and Spectral Analysis. *AJ* **2023**, *166*, 78, [arXiv:astro-ph.SR/2307.04926]. <https://doi.org/10.3847/1538-3881/ace59d>.
83. Anugu, N.; Gies, D.R.; Roettenbacher, R.M.; Monnier, J.D.; Montargés, M.; Mérand, A.; Baron, F.; Schaefer, G.H.; Shepard, K.A.; Kraus, S.; et al. Time Evolution Images of the Hypergiant RW Cephei during the Rebrightening Phase Following the Great Dimming. *ApJ* **2024**, *973*, L5, [arXiv:astro-ph.SR/2408.11906]. <https://doi.org/10.3847/2041-8213/ad736c>.
84. Noriega-Crespo, A.; van Buren, D.; Cao, Y.; Dgani, R. A Parsec-Size Bow Shock around Betelgeuse. *AJ* **1997**, *114*, 837–840. <https://doi.org/10.1086/118517>.
85. Cox, N.L.J.; Kerschbaum, F.; van Marle, A.J.; Decin, L.; Ladjal, D.; Mayer, A.; Groenewegen, M.A.T.; van Eck, S.; Royer, P.; Ottensamer, R.; et al. A far-infrared survey of bow shocks and detached shells around AGB stars and red supergiants. *A&A* **2012**, *537*, A35, [arXiv:astro-ph.GA/1110.5486]. <https://doi.org/10.1051/0004-6361/201117910>.
86. Gvaramadze, V.V.; Menten, K.M.; Kniazev, A.Y.; Langer, N.; Mackey, J.; Kraus, A.; Meyer, D.M.A.; Kamiński, T. IRC -10414: a bow-shock-producing red supergiant star. *MNRAS* **2014**, *437*, 843–856, [arXiv:astro-ph.SR/1310.2245]. <https://doi.org/10.1093/mnras/stt1943>.
87. Guarcello, M.G.; Almendros-Abad, V.; Lovell, J.B.; Monsch, K.; Mužić, K.; Martínez-Galarza, J.R.; Drake, J.J.; Anastasopoulou, K.; Andersen, M.; Argiroffi, C.; et al. EWOCS-III: JWST observations of the supermassive star cluster Westerlund 1. *A&A* **2025**, *693*, A120, [arXiv:astro-ph.SR/2411.13051]. <https://doi.org/10.1051/0004-6361/202452150>.
88. Munoz-Sanchez, G.; de Wit, S.; Bonanos, A.Z.; Antoniadis, K.; Boutsia, K.; Boumis, P.; Christodoulou, E.; Kalitsounaki, M.; Udalski, A. Episodic mass loss in the very luminous red supergiant [W60] B90 in the Large Magellanic Cloud. *A&A* **2024**, *690*, A99, [arXiv:astro-ph.SR/2405.11019]. <https://doi.org/10.1051/0004-6361/202450737>.
89. Beasor, E.R.; Davies, B.; Smith, N.; van Loon, J.T.; Gehrz, R.D.; Figer, D.F. A new mass-loss rate prescription for red supergiants. *MNRAS* **2020**, *492*, 5994–6006, [arXiv:astro-ph.SR/2001.07222]. <https://doi.org/10.1093/mnras/staa255>.
90. Decin, L.; Richards, A.M.S.; Marchant, P.; Sana, H. ALMA detection of CO rotational line emission in red supergiant stars of the massive young star cluster RSGC1. Determination of a new mass-loss rate prescription for red supergiants. *A&A* **2024**, *681*, A17, [arXiv:astro-ph.SR/2303.09385]. <https://doi.org/10.1051/0004-6361/202244635>.
91. Antoniadis, K.; Bonanos, A.Z.; de Wit, S.; Zapartas, E.; Munoz-Sanchez, G.; Maravelias, G. Establishing a mass-loss rate relation for red supergiants in the Large Magellanic Cloud. *A&A* **2024**, *686*, A88, [arXiv:astro-ph.SR/2401.15163]. <https://doi.org/10.1051/0004-6361/202449383>.
92. Kniazev, A.Y.; Grebel, E.K.; Pustilnik, S.A.; Pramskij, A.G.; Zucker, D.B. Spectrophotometry of Sextans A and B: Chemical Abundances of H II Regions and Planetary Nebulae. *AJ* **2005**, *130*, 1558–1573, [arXiv:astro-ph/astro-ph/0502562]. <https://doi.org/10.1086/432931>.

93. Urbaneja, M.A.; Kudritzki, R.P.; Bresolin, F.; Przybilla, N.; Gieren, W.; Pietrzyński, G. The Araucaria Project: The Local Group Galaxy WLM—Distance and Metallicity from Quantitative Spectroscopy of Blue Supergiants. *ApJ* **2008**, *684*, 118–135, [arXiv:astro-ph/0805.3555]. <https://doi.org/10.1086/590334>.
94. Zurita, A.; Bresolin, F. The chemical abundance in M31 from H II regions. *MNRAS* **2012**, *427*, 1463–1481, [arXiv:astro-ph.CO/1209.1505]. <https://doi.org/10.1111/j.1365-2966.2012.22075.x>.
95. Pietrzyński, G.; Graczyk, D.; Gallenne, A.; Gieren, W.; Thompson, I.B.; Pilecki, B.; Karczmarek, P.; Górski, M.; Suchomska, K.; Taormina, M.; et al. A distance to the Large Magellanic Cloud that is precise to one per cent. *Nature* **2019**, *567*, 200–203, [arXiv:astro-ph.GA/1903.08096]. <https://doi.org/10.1038/s41586-019-0999-4>.
96. Leavitt, H.S.; Pickering, E.C. Periods of 25 Variable Stars in the Small Magellanic Cloud. *Harvard College Observatory Circular* **1912**, *173*, 1–3.
97. Lee, M.G.; Freedman, W.L.; Madore, B.F. The Tip of the Red Giant Branch as a Distance Indicator for Resolved Galaxies. *ApJ* **1993**, *417*, 553. <https://doi.org/10.1086/173334>.
98. Bonanos, A.Z.; Stanek, K.Z.; Kudritzki, R.P.; Macri, L.M.; Sasselov, D.D.; Kaluzny, J.; Stetson, P.B.; Bersier, D.; Bresolin, F.; Matheson, T.; et al. The First DIRECT Distance Determination to a Detached Eclipsing Binary in M33. *ApJ* **2006**, *652*, 313–322, [arXiv:astro-ph/astro-ph/0606279]. <https://doi.org/10.1086/508140>.
99. Massey, P.; Olsen, K.A.G.; Hodge, P.W.; Strong, S.B.; Jacoby, G.H.; Schlingman, W.; Smith, R.C. A Survey of Local Group Galaxies Currently Forming Stars. I. UVRI Photometry of Stars in M31 and M33. *AJ* **2006**, *131*, 2478–2496, [arXiv:astro-ph/astro-ph/0602128]. <https://doi.org/10.1086/503256>.
100. Levesque, E.M.; Massey, P.; Olsen, K.A.G.; Plez, B.; Meynet, G.; Maeder, A. The Effective Temperatures and Physical Properties of Magellanic Cloud Red Supergiants: The Effects of Metallicity. *ApJ* **2006**, *645*, 1102–1117, [arXiv:astro-ph/astro-ph/0603596]. <https://doi.org/10.1086/504417>.
101. de Wit, S.; Bonanos, A.Z.; Tramper, F.; Yang, M.; Maravelias, G.; Boutsia, K.; Britavskiy, N.; Zapartas, E. Properties of luminous red supergiant stars in the Magellanic Clouds. *A&A* **2023**, *669*, A86, [arXiv:astro-ph.SR/2209.11239]. <https://doi.org/10.1051/0004-6361/20224339410.48550/arXiv.2209.11239>.
102. Massey, P.; Evans, K.A. The Red Supergiant Content of M31*. *ApJ* **2016**, *826*, 224, [arXiv:astro-ph.SR/1605.07900]. <https://doi.org/10.3847/0004-637X/826/2/224>.
103. Drout, M.R.; Massey, P.; Meynet, G. The Yellow and Red Supergiants of M33. *ApJ* **2012**, *750*, 97, [arXiv:astro-ph.SR/1203.0247]. <https://doi.org/10.1088/0004-637X/750/2/97>.
104. Britavskiy, N.E.; Bonanos, A.Z.; Mehner, A.; et al. Identification of red supergiants in nearby galaxies with mid-IR photometry. *A&A* **2014**, *562*, A75, [arXiv:astro-ph.SR/1309.6320]. <https://doi.org/10.1051/0004-6361/201322709>.
105. Britavskiy, N.E.; Bonanos, A.Z.; Herrero, A.; Cerviño, M.; García-Álvarez, D.; Boyer, M.L.; Masseron, T.; Mehner, A.; McQuinn, K.B.W. Physical parameters of red supergiants in dwarf irregular galaxies in the Local Group. *A&A* **2019**, *631*, A95, [arXiv:astro-ph.SR/1909.13378]. <https://doi.org/10.1051/0004-6361/201935212>.
106. González-Torà, G.; Davies, B.; Kudritzki, R.P.; Plez, B. The temperatures of red supergiants in low-metallicity environments. *MNRAS* **2021**, *505*, 4422–4443, [arXiv:astro-ph.GA/2106.01807]. <https://doi.org/10.1093/mnras/stab1611>.
107. Yang, M.; Bonanos, A.Z.; Jiang, B.W.; et al. Evolved massive stars at low metallicity. II. Red supergiant stars in the Small Magellanic Cloud. *A&A* **2020**, *639*, A116, [arXiv:astro-ph.SR/2005.10108]. <https://doi.org/10.1051/0004-6361/201937168>.
108. Yang, M.; Bonanos, A.Z.; Jiang, B.; Zapartas, E.; Gao, J.; Ren, Y.; Lam, M.I.; Wang, T.; Maravelias, G.; Gavras, P.; et al. Evolved massive stars at low-metallicity. V. Mass-loss rate of red supergiant stars in the Small Magellanic Cloud. *A&A* **2023**, *676*, A84, [arXiv:astro-ph.SR/2304.01835]. <https://doi.org/10.1051/0004-6361/202244770>.
109. Ren, Y.; Jiang, B.; Yang, M.; et al. The Sample of Red Supergiants in 12 Low-mass Galaxies of the Local Group. *ApJ* **2021**, *923*, 232, [arXiv:astro-ph.GA/2110.08793]. <https://doi.org/10.3847/1538-4357/ac307b>.
110. Antoniadis, K.; Zapartas, E.; Bonanos, A.Z.; Maravelias, G.; Vlassis, S.; Munoz-Sanchez, G.; Nally, C.; Meixner, M.; Jones, O.C.; Lenkic, L.; et al. Investigating the metallicity dependence of the mass-loss rate relation of red supergiants. *A&A, subm.* **2025**, [arXiv:astro-ph.SR/2503.05876]. <https://doi.org/10.48550/arXiv.2503.05876>.
111. Nally, C.; Jones, O.C.; Lenkic, L.; Habel, N.; Hirschauer, A.S.; Meixner, M.; Kavanagh, P.J.; Boyer, M.L.; Ferguson, A.M.N.; Sargent, B.A.; et al. JWST MIRI and NIRCам unveil previously unseen infrared stellar populations in NGC 6822. *MNRAS* **2024**, *531*, 183–198, [arXiv:astro-ph.GA/2309.13521]. <https://doi.org/10.1093/mnras/stae1163>.
112. Massey, P.; Neugent, K.F.; Levesque, E.M.; Drout, M.R.; Courteau, S. The Red Supergiant Content of M31 and M33. *AJ* **2021**, *161*, 79, [arXiv:astro-ph.SR/2011.13279]. <https://doi.org/10.3847/1538-3881/abd01f>.
113. Ren, Y.; Jiang, B.; Yang, M.; Wang, T.; Jian, M.; Ren, T. Red Supergiants in M31 and M33. I. The Complete Sample. *ApJ* **2021**, *907*, 18, [arXiv:astro-ph.SR/2011.12051]. <https://doi.org/10.3847/1538-4357/abcda5>.
114. Gazak, J.Z.; Kudritzki, R.; Evans, C.; Patrick, L.; Davies, B.; Bergemann, M.; Plez, B.; Bresolin, F.; Bender, R.; Wegner, M.; et al. Red Supergiants as Cosmic Abundance Probes: The Sculptor Galaxy NGC 300. *ApJ* **2015**, *805*, 182, [arXiv:astro-ph.GA/1505.00871]. <https://doi.org/10.1088/0004-637X/805/2/182>.
115. Patrick, L.R.; Evans, C.J.; Davies, B.; et al. Physical properties of the first spectroscopically confirmed red supergiant stars in the Sculptor Group galaxy NGC 55. *MNRAS* **2017**, *468*, 492–500, [arXiv:astro-ph.GA/1702.06966]. <https://doi.org/10.1093/mnras/stx410>.

116. Williams, S.J.; Bonanos, A.Z.; Whitmore, B.C.; Prieto, J.L.; Blair, W.P. The infrared massive stellar content of M 83. *A&A* **2015**, *578*, A100, [arXiv:astro-ph.SR/1503.05942]. <https://doi.org/10.1051/0004-6361/201525696>.
117. Davies, B.; Kudritzki, R.P.; Figer, D.F. The potential of red supergiants as extragalactic abundance probes at low spectral resolution. *MNRAS* **2010**, *407*, 1203–1211, [arXiv:astro-ph.CO/1005.1008]. <https://doi.org/10.1111/j.1365-2966.2010.16965.x>.
118. Davies, B.; Kudritzki, R.P.; Lardo, C.; Bergemann, M.; Beasor, E.; Plez, B.; Evans, C.; Bastian, N.; Patrick, L.R. Red Supergiants as Cosmic Abundance Probes: Massive Star Clusters in M83 and the Mass-Metallicity Relation of Nearby Galaxies. *ApJ* **2017**, *847*, 112, [arXiv:astro-ph.GA/1708.08948]. <https://doi.org/10.3847/1538-4357/aa89ed>.
119. Lardo, C.; Davies, B.; Kudritzki, R.P.; Gazak, J.Z.; Evans, C.J.; Patrick, L.R.; Bergemann, M.; Plez, B. Red Supergiants as Cosmic Abundance Probes: The First Direct Metallicity Determination of NGC 4038 in the Antennae. *ApJ* **2015**, *812*, 160, [arXiv:astro-ph.GA/1509.04937]. <https://doi.org/10.1088/0004-637X/812/2/160>.
120. Chun, S.H.; Sohn, Y.J.; Asplund, M.; Casagrande, L. Red supergiant stars in NGC 4449, NGC 5055 (M63) and NGC 5457 (M101). *MNRAS* **2017**, *467*, 102–114. <https://doi.org/10.1093/mnras/stx013>.
121. Elias, J.H.; Frogel, J.A.; Humphreys, R.M. M supergiants in the Milky Way and the Magellanic Clouds :colors, spectral types, and luminosities. *ApJS* **1985**, *57*, 91–131. <https://doi.org/10.1086/190997>.
122. Davies, B.; Kudritzki, R.P.; Plez, B.; Trager, S.; Lançon, A.; Gazak, Z.; Bergemann, M.; Evans, C.; Chiavassa, A. The Temperatures of Red Supergiants. *ApJ* **2013**, *767*, 3, [arXiv:astro-ph.SR/1302.2674]. <https://doi.org/10.1088/0004-637X/767/1/3>.
123. Davies, B.; Plez, B. The impact of winds on the spectral appearance of red supergiants. *MNRAS* **2021**, *508*, 5757–5765, [arXiv:astro-ph.SR/2109.05884]. <https://doi.org/10.1093/mnras/stab2645>.
124. Massey, P.; Levesque, E.M.; Olsen, K.A.G.; Plez, B.; Skiff, B.A. HV 11423: The Coolest Supergiant in the SMC. *ApJ* **2007**, *660*, 301–310, [arXiv:astro-ph/0701769]. <https://doi.org/10.1086/513182>.
125. Levesque, E.M.; Massey, P.; Olsen, K.A.G.; Plez, B. Late-Type Red Supergiants: Too Cool for the Magellanic Clouds? *ApJ* **2007**, *667*, 202–212, [arXiv:astro-ph/0705.3431]. <https://doi.org/10.1086/520797>.
126. Davies, B.; Kudritzki, R.P.; Gazak, Z.; Plez, B.; Bergemann, M.; Evans, C.; Patrick, L. Red Supergiants as Cosmic Abundance Probes: The Magellanic Clouds. *ApJ* **2015**, *806*, 21, [arXiv:astro-ph.GA/1504.03694]. <https://doi.org/10.1088/0004-637X/806/1/21>.
127. Patrick, L.R.; Evans, C.J.; Davies, B.; Kudritzki, R.P.; Gazak, J.Z.; Bergemann, M.; Plez, B.; Ferguson, A.M.N. Red Supergiant Stars as Cosmic Abundance Probes: KMOS Observations in NGC 6822. *ApJ* **2015**, *803*, 14, [arXiv:astro-ph.SR/1501.07601]. <https://doi.org/10.1088/0004-637X/803/1/14>.
128. Meynet, G.; Chomienne, V.; Ekström, S.; et al. Impact of mass-loss on the evolution and pre-supernova properties of red supergiants. *A&A* **2015**, *575*, A60, [arXiv:astro-ph.SR/1410.8721]. <https://doi.org/10.1051/0004-6361/201424671>.
129. Zapartas, E.; de Wit, S.; Antoniadis, K.; Muñoz-Sanchez, G.; Souropanis, D.; Bonanos, A.Z.; Maravelias, G.; Kovelakas, K.; Kruckow, M.U.; Fragos, T.; et al. The effect of mass loss in models of red supergiants in the Small Magellanic Cloud. *A&A* **2025**, *697*, A167, [arXiv:astro-ph.SR/2410.07335]. <https://doi.org/10.1051/0004-6361/202452401>.
130. Humphreys, R.M.; Helmelt, G.; Jones, T.J.; Gordon, M.S. Exploring the Mass-loss Histories of the Red Supergiants. *AJ* **2020**, *160*, 145, [arXiv:astro-ph.SR/2008.01108]. <https://doi.org/10.3847/1538-3881/abab15>.
131. Neugent, K.F.; Massey, P.; Georgy, C.; Drout, M.R.; Mommert, M.; Levesque, E.M.; Meynet, G.; Ekström, S. The Luminosity Function of Red Supergiants in M31. *ApJ* **2020**, *889*, 44, [arXiv:astro-ph.SR/1911.10638]. <https://doi.org/10.3847/1538-4357/ab5ba0>.
132. Massey, P.; Neugent, K.F.; Ekström, S.; et al. The Time-averaged Mass-loss Rates of Red Supergiants as Revealed by Their Luminosity Functions in M31 and M33. *ApJ* **2023**, *942*, 69, [arXiv:astro-ph.SR/2211.14147]. <https://doi.org/10.3847/1538-4357/aca66510.48550/arXiv.2211.14147>.
133. Gordon, M.S.; Humphreys, R.M.; Jones, T.J. Luminous and Variable Stars in M31 and M33. III. The Yellow and Red Supergiants and Post-red Supergiant Evolution. *ApJ* **2016**, *825*, 50, [arXiv:astro-ph.SR/1603.08003]. <https://doi.org/10.3847/0004-637X/825/1/50>.
134. Davies, B.; Crowther, P.A.; Beasor, E.R. The luminosities of cool supergiants in the Magellanic Clouds, and the Humphreys-Davidson limit revisited. *MNRAS* **2018**, *478*, 3138–3148, [arXiv:astro-ph.SR/1804.06417]. <https://doi.org/10.1093/mnras/sty1302>.
135. McDonald, S.L.E.; Davies, B.; Beasor, E.R. Red supergiants in M31: the Humphreys-Davidson limit at high metallicity. *MNRAS* **2022**, *510*, 3132–3144, [arXiv:astro-ph.GA/2111.13716]. <https://doi.org/10.1093/mnras/stab3453>.
136. Martin, J.C.; Humphreys, R.M. A Census of the Most Luminous Stars. I. The Upper HR Diagram for the Large Magellanic Cloud. *AJ* **2023**, *166*, 214. <https://doi.org/10.3847/1538-3881/ad011e>.
137. Ohnaka, K.; Hofmann, K.H.; Weigelt, G.; van Loon, J.T.; Schertl, D.; Goldman, S.R. Imaging the innermost circumstellar environment of the red supergiant WOH G64 in the Large Magellanic Cloud. *A&A* **2024**, *691*, L15, [arXiv:astro-ph.SR/2412.01921]. <https://doi.org/10.1051/0004-6361/202451820>.
138. Smith, N. Mass Loss: Its Effect on the Evolution and Fate of High-Mass Stars. *ARA&A* **2014**, *52*, 487–528, [arXiv:astro-ph.SR/1402.1237]. <https://doi.org/10.1146/annurev-astro-081913-040025>.
139. Muñoz-Sanchez, G.; Kalitsounaki, M.; de Wit, S.; Antoniadis, K.; Bonanos, A.Z.; Zapartas, E.; Boutsia, K.; Christodoulou, E.; Maravelias, G.; Soszynski, I.; et al. The dramatic transition of the extreme Red Supergiant WOH G64 to a Yellow Hypergiant. *arXiv e-prints* **2024**, p. arXiv:2411.19329, [arXiv:astro-ph.SR/2411.19329]. <https://doi.org/10.48550/arXiv.2411.19329>.
140. Ohnaka, K.; Driebe, T.; Hofmann, K.H.; Weigelt, G.; Wittkowski, M. Spatially resolved dusty torus toward the red supergiant WOH G64 in the Large Magellanic Cloud. *A&A* **2008**, *484*, 371–379, [arXiv:astro-ph/0803.3823]. <https://doi.org/10.1051/0004-6361:200809469>.

141. Beasor, E.R.; Smith, N. The Extreme Scarcity of Dust-enshrouded Red Supergiants: Consequences for Producing Stripped Stars via Winds. *ApJ* **2022**, *933*, 41, [arXiv:astro-ph.SR/2205.02207]. <https://doi.org/10.3847/1538-4357/ac6dcf>.
142. Humphreys, R.M.; Jones, T.J.; Polomski, E.; et al. M33's Variable A: A Hypergiant Star More Than 35 YEARS in Eruption. *AJ* **2006**, *131*, 2105–2113, [arXiv:astro-ph/astro-ph/0601116]. <https://doi.org/10.1086/500811>.
143. Levesque, E.M. *Astrophysics of Red Supergiants*; 2017. <https://doi.org/10.1088/978-0-7503-1329-2>.
144. Yang, M.; Jiang, B.W. Red Supergiant Stars in the Large Magellanic Cloud. I. The Period-Luminosity Relation. *ApJ* **2011**, *727*, 53, [arXiv:astro-ph.SR/1011.4998]. <https://doi.org/10.1088/0004-637X/727/1/53>.
145. Goldberg, J.A.; Joyce, M.; Molnár, L. A Buddy for Betelgeuse: Binarity as the Origin of the Long Secondary Period in α Orionis. *ApJ* **2024**, *977*, 35, [arXiv:astro-ph.SR/2408.09089]. <https://doi.org/10.3847/1538-4357/ad87f4>.
146. Humphreys, R.M.; Davidson, K.; Richards, A.M.S.; Ziurys, L.M.; Jones, T.J.; Ishibashi, K. The Mass-loss History of the Red Hypergiant VY CMa. *AJ* **2021**, *161*, 98, [arXiv:astro-ph.SR/2012.08550]. <https://doi.org/10.3847/1538-3881/abd316>.
147. Jencson, J.E.; Sand, D.J.; Andrews, J.E.; Smith, N.; Pearson, J.; Strader, J.; Valenti, S.; Beasor, E.R.; Rothberg, B. An Exceptional Dimming Event for a Massive, Cool Supergiant in M51. *ApJ* **2022**, *930*, 81, [arXiv:astro-ph.SR/2110.11376]. <https://doi.org/10.3847/1538-4357/ac626c>.
148. Sana, H.; de Mink, S.E.; de Koter, A.; Langer, N.; Evans, C.J.; Gieles, M.; Gosset, E.; Izzard, R.G.; Le Bouquin, J.B.; Schneider, F.R.N. Binary Interaction Dominates the Evolution of Massive Stars. *Science* **2012**, *337*, 444, [arXiv:astro-ph.SR/1207.6397]. <https://doi.org/10.1126/science.1223344>.
149. Neugent, K.F.; Levesque, E.M.; Massey, P.; Morrell, N.I. Binary Red Supergiants. II. Discovering and Characterizing B-type Companions. *ApJ* **2019**, *875*, 124, [arXiv:astro-ph.SR/1903.06181]. <https://doi.org/10.3847/1538-4357/ab1012>.
150. Neugent, K.F.; Levesque, E.M.; Massey, P.; Morrell, N.I.; Drout, M.R. The Red Supergiant Binary Fraction of the Large Magellanic Cloud. *ApJ* **2020**, *900*, 118, [arXiv:astro-ph.SR/2007.15852]. <https://doi.org/10.3847/1538-4357/ababaa>.
151. González-Fernández, C.; Dorda, R.; Negueruela, I.; Marco, A. A new survey of cool supergiants in the Magellanic Clouds. *A&A* **2015**, *578*, A3, [arXiv:astro-ph.SR/1504.00003]. <https://doi.org/10.1051/0004-6361/201425362>.
152. Neugent, K.F.; Levesque, E.M.; Massey, P. Binary Red Supergiants: A New Method for Detecting B-type Companions. *AJ* **2018**, *156*, 225, [arXiv:astro-ph.SR/1809.10071]. <https://doi.org/10.3847/1538-3881/aae4e0>.
153. Neugent, K.F. The Red Supergiant Binary Fraction as a Function of Metallicity in M31 and M33. *ApJ* **2021**, *908*, 87, [arXiv:astro-ph.GA/2012.08531]. <https://doi.org/10.3847/1538-4357/abd47b>.
154. Patrick, L.R.; Thilker, D.; Lennon, D.J.; Bianchi, L.; Schootemeijer, A.; Dorda, R.; Langer, N.; Negueruela, I. Red supergiant stars in binary systems. I. Identification and characterization in the small magellanic cloud from the UVIT ultraviolet imaging survey. *MNRAS* **2022**, *513*, 5847–5860, [arXiv:astro-ph.SR/2204.11866]. <https://doi.org/10.1093/mnras/stac1139>.
155. Patrick, L.R.; Lennon, D.J.; Schootemeijer, A.; Bianchi, L.; Negueruela, I.; Langer, N.; Thilker, D.; Dorda, R. Red supergiant stars in binary systems II. Confirmation of B-type companions of red supergiants in the Small Magellanic Cloud using Hubble ultra-violet spectroscopy. *arXiv e-prints* **2024**, p. arXiv:2412.18554, [arXiv:astro-ph.SR/2412.18554]. <https://doi.org/10.48550/arXiv.2412.18554>.
156. MacLeod, M.; Blunt, S.; De Rosa, R.J.; Dupree, A.K.; Granzer, T.; Harper, G.M.; Huang, C.D.; Leiner, E.M.; Loeb, A.; Nielsen, E.L.; et al. Radial Velocity and Astrometric Evidence for a Close Companion to Betelgeuse. *ApJ* **2025**, *978*, 50, [arXiv:astro-ph.SR/2409.11332]. <https://doi.org/10.3847/1538-4357/ad93c8>.
157. Levesque, E.M.; Massey, P.; Zytzkow, A.N.; Morrell, N. Discovery of a Thorne-Zytzkow object candidate in the Small Magellanic Cloud. *MNRAS* **2014**, *443*, L94–L98, [arXiv:astro-ph.SR/1406.0001]. <https://doi.org/10.1093/mnrasl/slu080>.
158. DeMarchi, L.; Sanders, J.R.; Levesque, E.M. Prospects for Multimessenger Observations of Thorne-Zytzkow Objects. *ApJ* **2021**, *911*, 101, [arXiv:astro-ph.HE/2103.03887]. <https://doi.org/10.3847/1538-4357/abebe1>.
159. Britavskiy, N.; Lennon, D.J.; Patrick, L.R.; Evans, C.J.; Herrero, A.; Langer, N.; van Loon, J.T.; Clark, J.S.; Schneider, F.R.N.; Almeida, L.A.; et al. The VLT-FLAMES Tarantula Survey. XXX. Red stragglers in the clusters Hodge 301 and SL 639. *A&A* **2019**, *624*, A128, [arXiv:astro-ph.SR/1902.09891]. <https://doi.org/10.1051/0004-6361/201834564>.
160. Beasor, E.R.; Davies, B.; Smith, N.; Bastian, N. Discrepancies in the ages of young star clusters; evidence for mergers? *MNRAS* **2019**, *486*, 266–273, [arXiv:astro-ph.SR/1903.05106]. <https://doi.org/10.1093/mnras/stz732>.
161. Patrick, L.R.; Lennon, D.J.; Evans, C.J.; Sana, H.; Bodensteiner, J.; Britavskiy, N.; Dorda, R.; Herrero, A.; Negueruela, I.; de Koter, A. Multiplicity of the red supergiant population in the young massive cluster NGC 330. *A&A* **2020**, *635*, A29, [arXiv:astro-ph.SR/2001.02700]. <https://doi.org/10.1051/0004-6361/201936741>.
162. Wang, C.; Patrick, L.; Schootemeijer, A.; de Mink, S.E.; Langer, N.; Britavskiy, N.; Xu, X.T.; Bodensteiner, J.; Laplace, E.; Valli, R.; et al. Using Detailed Single-star and Binary-evolution Models to Probe the Large Observed Luminosity Spread of Red Supergiants in Young Open Star Clusters. *ApJ* **2025**, *981*, L16, [arXiv:astro-ph.SR/2502.13642]. <https://doi.org/10.3847/2041-8213/adb61a>.
163. Freytag, B.; Steffen, M.; Ludwig, H.G.; Wedemeyer-Böhm, S.; Schaffenberger, W.; Steiner, O. Simulations of stellar convection with CO5BOLD. *Journal of Computational Physics* **2012**, *231*, 919–959, [arXiv:astro-ph.SR/1110.6844]. <https://doi.org/10.1016/j.jcp.2011.09.026>.
164. Ma, J.Z.; Chiavassa, A.; de Mink, S.E.; Valli, R.; Justham, S.; Freytag, B. Is Betelgeuse Really Rotating? Synthetic ALMA Observations of Large-scale Convection in 3D Simulations of Red Supergiants. *ApJ* **2024**, *962*, L36, [arXiv:astro-ph.SR/2311.16885]. <https://doi.org/10.3847/2041-8213/ad24fd>.

165. Fragos, T.; Andrews, J.J.; Bavera, S.S.; Berry, C.P.L.; Coughlin, S.; Dotter, A.; Giri, P.; Kalogera, V.; Katsaggelos, A.; Kovelakas, K.; et al. POSYDON: A General-purpose Population Synthesis Code with Detailed Binary-evolution Simulations. *ApJS* **2023**, *264*, 45, [arXiv:astro-ph.SR/2202.05892]. <https://doi.org/10.3847/1538-4365/ac90c1>.
166. Andrews, J.J.; Bavera, S.S.; Briel, M.; Chattaraj, A.; Dotter, A.; Fragos, T.; Gallegos-Garcia, M.; Gossage, S.; Kalogera, V.; Kasdagli, E.; et al. POSYDON Version 2: Population Synthesis with Detailed Binary-Evolution Simulations across a Cosmological Range of Metallicities. *arXiv e-prints* **2024**, p. arXiv:2411.02376, [arXiv:astro-ph.GA/2411.02376]. <https://doi.org/10.48550/arXiv.2411.02376>.

Disclaimer/Publisher's Note: The statements, opinions and data contained in all publications are solely those of the individual author(s) and contributor(s) and not of MDPI and/or the editor(s). MDPI and/or the editor(s) disclaim responsibility for any injury to people or property resulting from any ideas, methods, instructions or products referred to in the content.